# STUDY OF ISOTHERMAL MULTIEXPONENTIAL TRANSIENTS FROM DEEPLEVELS IN SEMICONDUCTORS

A Thesis Submitted
In Partial Fulfilment of the Requirements
for the Degree of

## MASTER OF TECHNOLOGY

by
**ASHUTOSH RAZDAN**

to the

**DEPARTMENT OF ELECTRICAL ENGINEERING**
INDIAN INSTITUTE OF TECHNOLOGY, KANPUR
SEPTEMBER 1984

# CERTIFICATE

This is to certify that the thesis entitled 'STUDY OF ISOTHERMAL MULTIEXPONENTIAL TRANSIENTS FROM DEEP LEVEL IMPURITIES IN SEMICONDUCTORS' is a record of work carried out by Shri Ashutosh Razdan, Roll No. 8210404 under my supervision and that it has not been submitted elsewhere for a degree.

( R. Sharan )
Professor
Department of Electrical Engineeri
Indian Institute of Technology
Kanpur

EE- ☒ 1904- M - RAZ - STU

Dedicated

to

Tathaji and Amma

## ACKNOWLEDGEMENTS

# ABSTRACT

This work deals with characterization of deep level impurities, particularly of Gold in silicon. Isothermal relaxation data, using space charge spectroscopic principles, has been obtained, using set ups to measure low level capacitance and current signals from the device. Both single shot and synchronous detection methods of measurement and analysis have been used. The problem of det. of multi-exponential transients, which has been eluding an accurate and reliable solution, has been treated using an appropriate signal processing algorithm. In the present work the acquisition and analysis functions, which are performed simultaneously in the classical deep level transient spectroscopy (DLTS) developed by Lang, have been separated. This separation has been achieved using transient recording and analysis on a signal analyser, whose large memory as well as facilities for development of various analysis and signal processing routines have been found of immense use in analysis. The results have been obtained on a commercial $P^+N$ Jn diode 1N4148, for which the other relevant data was readily available. Important parameters such as activation energy and capture cross-sections have been determined.

# TABLE OF CONTENTS

# CHAPTER 1

## INTRODUCTION

Deep levels in semiconductors play an important role in device performance. They determine crucial device parameters as mean lifetime, activation energy, recombination efficiency etc. Hence it is essential to accurately characterize deep levels. This, however, is not a simple process, essentially because deep levels can get created not only when a known impurity is added but also they get inadvertently created due to lattice defects. The presence of one can affect the performance of the other deep levels as a recombination center. For instance Gold is extensively used in semiconductor industry for fast switching operations and lot of data on its parameters has been reported in literature. The reported values, however, vary by orders of magnitude. Wu and Peaker [16] have reported a survey of these values over the years. Table 1.1 just lists the electron cross-section values of Gold acceptor in silicon. This clearly suggests a degree of unpredictability related to values of Gold parameters. This unpredictability is partly justified by Bullis [9], wherein these parameters are found dependent upon several factors like the characteristics of initial material,

Table 1.1: Electron cross-section of Gold acceptor in
silicon.

| Author | Year | $\sigma_n(cm^2)$ | Temp(K) | Material | Technique |
|---|---|---|---|---|---|
| Bemski and Struthers | 1958 | $5 \times 10^{-16}$ | 200-450 | $N_T = N_D$ | Minority Lifetime |
| Davies | 1959 | $2 \times 10^{-15}$ | 77 | CZ $N_T \gg N_D$ | Majority Lifetime |
| Fairfield and Gokhale | 1965 | $8.4 \times 10^{-17}$ | 300 | CZ $N_T = 0.1 N_D$ | P.C. Decay |
| Senechal and Basinski | 1968 | $2.5 \times 10^{-15}$ | 250 | CZ $N_T = N_D$ | Junc. Cap. |
| Sah et.al. | 1970 | $2 \times 10^{-16}$ | 80 | $N_T = 0.3 N_D$ | Maj. Flux junc. cap. |
| Zohta | 1972 | $4.6 \times 10^{-15}$ | 300 | FZ $N_T = N_D$ | Junc. Cap. |
| Kassing and Lenz | 1974 | $8.3 \times 10^{-15}$ | 300 | $n^+ i\, n^+ N_T \gg N_D$ | SCLC |
| Pals | 1974 | $1.3 \times 10^{-16}$ | 77-220 | CZ $N_T = 0.2 N_D$ | Pulse/Junc. cap. |
| Nagasawa and Schultz | 1975 | $2.2 \times 10^{-15}$ | 300 | Implanted | Pulse/Junc. Cap. |
| Kassing et.al. | 1975 | $7.3 \times 10^{-14}$ | 172-316 | $n^+ i\, n^+ N_T \gg N_D$ | SCLC |
| Barbolla et.al. | 1976 | $8.3 \times 10^{-17}$ | 80-205 | CZ $N_T = 0.3 N_D$ | Pulse/Junc. Cap. |
| Dudeck and Kassing | 1977 | $1.5 \times 10^{-15}$ | 300 | $n^+ i\, n^+ N_T \gg N_D$ | SCLC |
| Brotherton and Bicknall | 1978 | $9.10^{-17}$ | 77-280 | CZ $N_T = 0.1 N_D$ | Pulse/Junc.Ca |
| Nassibian and Farone | 1978 | $1.10^{-15}$ | 235-265 | | Minority/life |
| Lang et.al | 1980 | $6.9 \times 10^{-17}$ | 295 | EPI $N_T < 0.1 N_D$ | Pulse/Junc.Ca |
| Lang et.al. | 1980 | $1.7 \times 10^{-16}$ | 115-424 | CZ $N_T = 0.1 N_D$ | Pulse/Junc.ca |
| Wu and Peaker | 1981 | $8.5 \times 10^{-17}$ | 80-200 | CZ $N_T\, 0.1 N_D$ | Pulse/Junc.ca |

behaviour of one type of deep level in presence of another deep level or even the shallow levels. Lang [ 10 ]has conclude that in place of a well defined unique level, there are family o closely related but different gold based complexes.

This work concentrates on Gold in silicon. The deep level impurity characterization can be done using either isothermal or nonisothermal relaxation. Here the former method is chosen and in particular, junction spectroscopic methods have been used. These methods have the advantage that one can distinguish between electron and hole traps and further one can get directly, emission rates and related data. Both single shot and synchronous methods of analyses have been used. They are detailed in Chapter 2. Chapter 2 also includes the theory behind current and capacitance transients as tools to deep level characterization using isothermal junction transient methods. Lang's method of Deep Level Transient spectroscopy (DLTS) is also explained in Chapter 2.

Chapter 3 discusses the analysis procedures for current and capacitance transients from the sample. It is found that this data is quite unamenable to accurate characterization because of two reasons, one that the transient has a steady state level on which it sits and two,

that instead of having single exponent, it can have a sum
of exponents (or multiexponent). Physically multiexponents
can mean that more than one trap are involved in recombination
process. The data in that case can be thought of having
form like $\sum_{i=1}^{n} A_i e^{-\alpha_i t}$ . The problem is to accurately
find values of $A_i$, n and $\alpha_i$. Apparently it looks a trivial
problem, which it is not [11]. According to Lanczos [11],
the practical solution of these problems is beset with
numerical difficulties. For an accurate determination, large
data accuracy is needed. If it is not so, one can get
totally unsatisfactory results. In no way, any of the least
square treatments can help retrieve the situation for insu-
fficiently accurate initial data. Chapter 3 goes into details
of these problems. Multiexponents have been extracted using
an appropriate signal processing algorithm due to Gardner
et.al. [12]. Chapter three contains the details of this
method and the reasons of its success. In the same chapter,
several other signal analysing algorithms are described.
They    deal with the determination of parameters in a single
exponential decay from the samples, in the presence of a
constant d.c. shift.

The    particular    method    of
DLTS suffers from the fact that analysis is done using

hardwired instruments and each point in Arrhenius plot requires one thermal scan. Obviously this is very time consuming and hence this work delineates it into two independent functions of acquisition and analysis. The details of Box-car programs in Appendix I,help in underlining the advantage of using one thermal scan and getting all what one could get from conventional DLTS.

Chapter 4 contains the details of measurement system used for characterizing the deep levels. The design of capacitance and current transient measurement modules is described in the same chapter. In both the cases, the signal is of low level in nature. The capacitance transient is, in particular, monitored by high frequency small signals.

Chapter 5 contains the experimental data taken on a commercial $P^+N$ junction diode 1N4148. Using the theory and analyses of second and third chapters, deep level parameters like activation energy and capture cross-section have been determined. Discussions of the results follow in the same chapter.

Chapter 6 contains the conclusion and suggestions for further improvements.

Appendix I and II contain program listings for analysis procedures described in Chapter 3.

As lot of data has been obtained from the signal analyser, a typical plot is explained briefly in Appendix III.

# CHAPTER 2

## ISOTHERMAL RELAXATION STUDY FOR DEEP LEVEL IMPURITIES

### 2.1 INTRODUCTION:

Current transport in semiconductors is determined by electrons and holes in conduction and valence bands respectively. The number of electrons in the conduction band or holes in the valence band is dependent upon the doping and the generation-recombination process in the semiconductor. At any instant these carriers can be generated either thermally or by any other external perturbation and they recombine with a mean life time. The process of recombination, particularly, is strongly dependent upon the impurities in the semiconductor. Hence efforts have been made to measure the parameters of the impurities (e.g. life time etc.) accurately and relate them to various device parameters like conductivity etc. The process of recombination can be band-to-band or band-to-impurity-to band. However theoretical values assuming only band to band transitions have been orders of magnitude different from experimental results in silicon and Germanium. Shockley et.al. [6] in their theory called SRH statistics explain the discrepancy in these 'indirect' materials by assuming the existence of one or

more **deep** levels within the band gap. These levels act
as recombination centres. Though this idea of the existence
of **deep** levels in SR$^H$ statistics was a theoretical
construct, subsequent experimentation has confirmed their
presence. Thus an accurate characterization of these
deep levels has helped solve two problems. One that the
above said discrepancy in values of mean lifetime has
been explained and secondly one can tailor device chara-
cteristics according to one's needs. The exact effect
of deep levels on recombination can be known from SRH
statistics. Here only those aspects of SRH statistics
will be discussed which are pertinent to our characteriza-
tion of deep levels.

Consider a deep level acting as a recombination
center within the band gap as shown in Fig. 2.1. The deep
level recombination center or trap can essentially:

1. capture electrons from conduction band $r_a$
2. emit electrons to conduction band $r_b$
3. capture holes from valence band $r_c$
4. emit holes to valence band $r_d$.

Let $\langle V \rangle$ be the mean thermal velocity

$\sigma_n, \sigma_p$   capture cross-sections for electrons
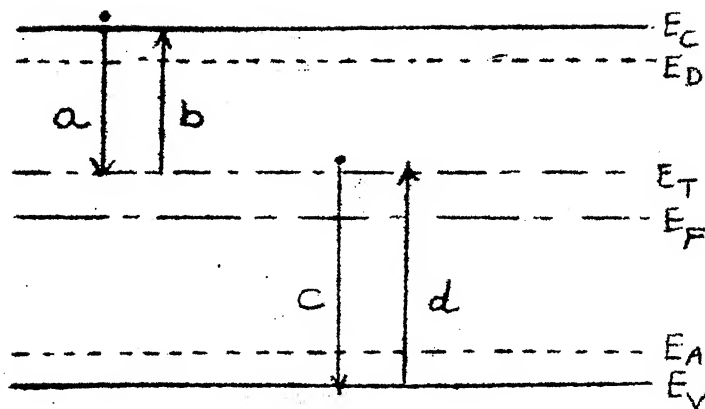and holes

$N_t$   the trap concentration

Fig. 2.1: Energy band diagram with a single trap level at $E_T$.

$e_n, e_p$ the emission rates of electrons and holes and

$$f = \frac{1}{1+e^{(E_t-E_F)/kT}}$$ be the probability that

a given trap level is occupied by an electron.

The rates of the above four processes $r_a, r_b, r_c$ and $r_d$ is given by

1. $r_a = \langle V \rangle \sigma_n n \cdot N_t (1-f)$         (2.1)

2. $r_b = e_n \cdot N_t \cdot f$         (2.2)

3. $r_c = \langle V \rangle \sigma_p \cdot p \cdot N_t \cdot f$         (2.3)

4. $r_d = e_p \cdot N_t (1-f)$         (2.4)

under thermal equilibrium

$$r_a = r_b \text{ and } r_c = r_d$$

From $r_a = r_b$ we have from eqn. (2.1) and (2.2)

$$\langle V \rangle \sigma_n \cdot n \cdot N_t (1-f) = e_n N_t \cdot f \qquad (2.5)$$

on solving eqn. (2.5) one gets for $e_n$

$$e_n = \langle V \rangle \sigma_n N_c e^{(E_t-E_c)/kT} \qquad (2.6)$$

similarly from $r_c = r_d$ one gets

$$e_p = \langle V \rangle \sigma_p N_v e^{(E_v-E_t)/kT} \qquad (2.7)$$

From eqns. (2.6) or (2.7), if one plots natural logarithm of $e_n$ or $e_p$ against 1/T, the resulting straight line gives the activation energy as slope and ordinate intercept provides capture cross-section. Such a plot called Arrhenius plot is used to characterize the deep level recombination centre. Hence methods, both direct and indirect, have been devised to get values of $e_n$ or $e_p$. In this analysis direct method using junction spectroscopic principles has been utilized. It has been found that the capacitance or current due to the deep level filling or emptying in the space-charge region is in the form of a transient and is related to emission rates of carriers and the trap concentration. Section 2.2 gives in detail the origin of the capacitance and current transients. The analysis of these transients can be done in several ways and are detailed in Section 2.3.

## 2.2 CAPACITANCE AND CURRENT TRANSIENTS AS PROBES TO RELAXATION STUDY:

Let $n_T$ and $p_T$ be the concentration of electrons and holes at the trap. From eqn. (2.1) and (2.2), the rate of change of electron concentration $(\frac{dn}{dt})_T$ in conduction band due to trap can be found as

$$( \frac{dn}{dt} )_T = r_b - r_a = e_n\, n_t - c_n\, n\, p_T \tag{2.8}$$

where $c_n = \langle V \rangle\, \sigma_n$

Similarly from eqns. (2.3) and (2.4), for rate of change of hole concentration $(\frac{dp}{dt})_T$ in valence band due to trap, can be written as:

$$( \frac{dp}{dt} )_T = r_d - r_c = e_p p_T - C_p\, p\, n_T \tag{2.9}$$

From eqns. (2.1), (2.2), (2.3) and (2.4), the rate of change of trap electron concentration $(\frac{dn_T}{dt})$ is as

$$(\frac{dn_T}{dt}) = r_a - r_b + r_d - r_c$$

$$= -(e_n + c_p p + c_n n + e_p)n_T$$

$$+ (e_p + c_n n)N_{TT} \tag{2.10}$$

where $N_{TT} = n_T + p_T =$ trap concentration. Solution of eqn. (2.10) yields within depletion region for $n = p = o$

$$n_T( t) = n_T(\infty) + [n_T(o) - n_T(\infty)]e^{-t/Z_{ON}} \tag{2.11}$$

where,

$$Z_{ON} = \frac{1}{e_n + e_p}$$

$n_T(\infty)$ is the final value and is given by

$$n_T(\infty) = N_{TT} ( \frac{e_p}{e_n + e_p} ) \tag{2.12}$$

$$\text{and} \quad n_T(o) = N_{TT} \left( \frac{N_E}{N_E + e_1} \right) \tag{2.13}$$

$$= N_{TT} \ (P^+N \ Jn)$$

$$= O \ (N^+P \ Jn)$$

where $N_E$ is the equilibrium concentration. From eqn. (2.11) one sees that trapped electron concentration decreases exponentially with time and hence within deplection region, the corresponding capacitance and current, too, will change according to trapped electron concentration.

A typical experiment to measure this capacitance or current transient involves application of a suitable voltage                        and observing the sample response. The response, however, is strongly dependent upon temperature. Therefore one does the experiment either at a constant temperature and hence iso-thermal measurements, or varies temperature according to a program and therefore nonisothermal measurements. This work uses isothermal conditions and the applied voltage is in the form of a pulse-bias. There are two types of pulses one can use. In one there is no carrier injection process in the sample and in another there is carrier injection. The former is called a majority carrier pulse while the latter is called minority carrier pulse. Each of

the pulses can be used to characterize majority and minority carrier traps respectively [5]. The effect of a pulse bias on filling and emptying process in $P^+N$ junction diode is shown in Fig. 2.2. The pulse used is a majority carrier pulse. In subsequent sections, both capacitance and current transient signal expressions will be derived for a majority carrier pulse in a $P^+N$ Jn.

### 2.2.2 Theory of Capacitance Transients:

The transition capacitance in a junction diode is given by $i = C_T \frac{dv}{dt}$. From Poisson's equation and its solution we get

$$V_j = \frac{qN_I W^2}{2\varepsilon} \qquad (2.14)$$

where W is the width of depletion region, $N_I$ the concentration of ionized impurities in it, $\varepsilon$ the permittivity within it and $V_j$ the junction potential.

From eqn. (2.14) and $C_T = \frac{\varepsilon A}{W}$ , one gets

$$C_T^2 = \frac{A^2 \varepsilon q N_I}{2V_j} \qquad (2.15)$$

For an acceptor level in a $P^+N$ junction, $N_I = N_D - n_T$ and hence eqn. (2.15) becomes

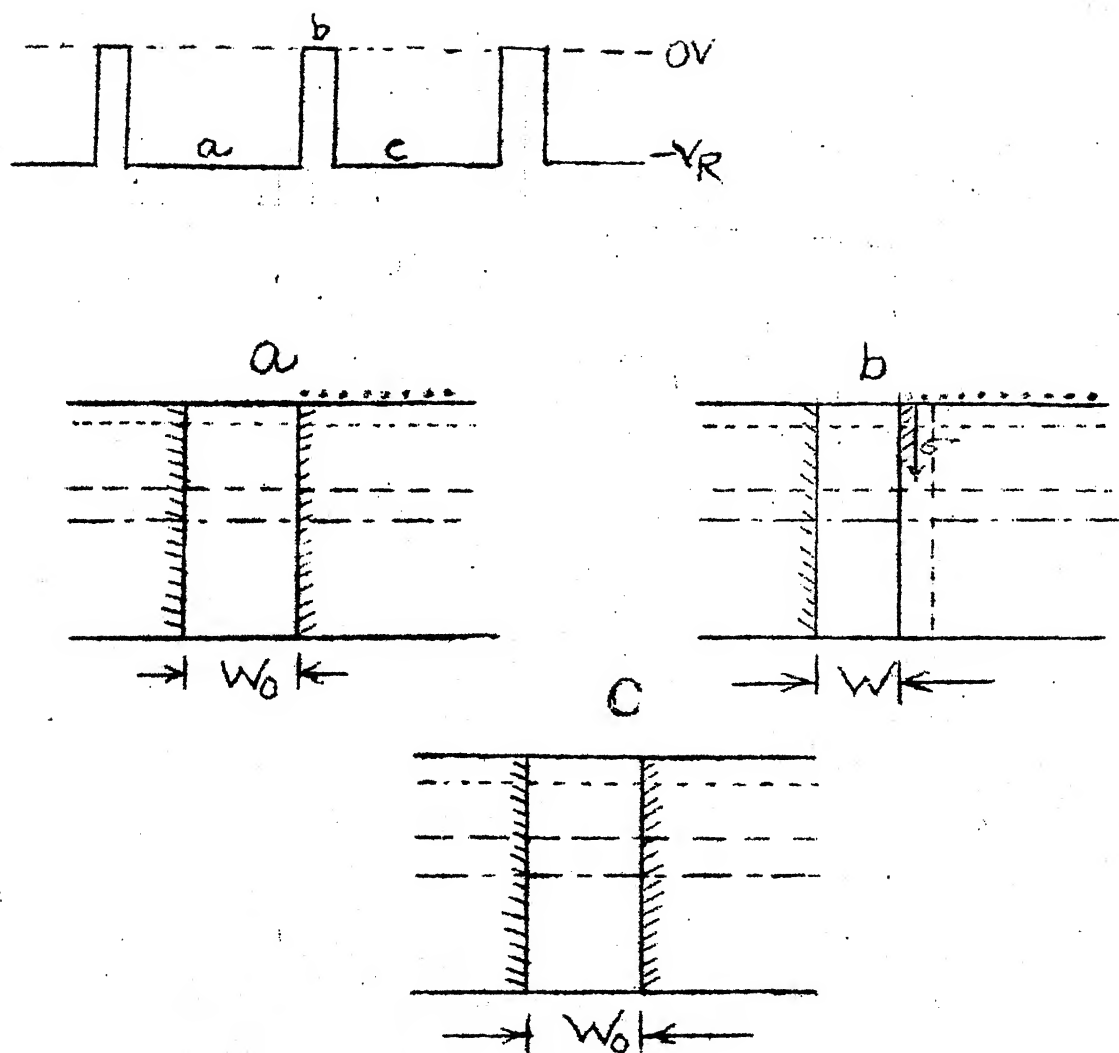$$C_T^2 = \frac{A^2 \varepsilon q}{2V_j} (N_D - n_T) \qquad (2.16)$$

Fig. 2.2: 1) Majority carrier pulse (2)-(4): Energy band diagram showing depletion region (with shaded lines) as well as capture, emission and trap occupation during the three states a,b and c of the majority carrier pulse.

or

$$C_T = C_m \left[ 1 - \frac{\Delta C(t)}{C_m} \right] \qquad (2.17)$$

where,

$$C_m = \frac{A^2 \, q \, N_D}{2V_j}$$

and

$$\frac{\Delta C(t)}{C_m} = \frac{n_T}{2N_D} \qquad (2.18)$$

Using eqn. (2.13) a and for acceptor level $e_n \gg e_p$, we get for (2.18)

$$\frac{C(t)}{C_m} = \frac{n_T(o)}{2N_D} e^{-t/\tau_n}$$

$$= \frac{N_{TT}}{2N_D} e^{-t/\tau_n} \qquad (2.19)$$

Thus capacitance transient from a majority carrier pulse gives value of $\tau_n$ directly. Using eqn. (2.6), one can obtain values of activation energy and capture cross-section. The initial value of transient has information regarding the trap concentration.

## 2.2.3 Theory of Current Transients:

The pulse sequence applied in this case, too, is as in Fig.2.2(1).As the voltage switches from 0 to $-V_R$, three components are obtained in the current transient signal.

1. A fast component in the form of a spike of very short duration is produced due to sweep out of majority carriers in the part of depletion region, which gets affected due to pulse bias sequence.

2. The slow current transient due to trap occupation has two forms. One consisting of conduction due to electrons and holes and other due to displacement currents, because of induced charge in x < o and x > w region, due to $\frac{dn_T}{dt}$ . The components of slow transient are shown in Figure 2.3.

The conduction current due to electrons

$$i_{c_n} = A \int_o^w q \left(\frac{dn}{dt}\right)_T dx$$

$$= A q \, e_n n_T(t) \, w(t) \qquad (2.20)$$

where A and w are area and width of junction respectively and n=o while using eq. (2.8).

3. The displacement current is given by

$$i_d(t) = A \int_o^w q\left(\frac{dn_T}{dt}\right) (x/w)dx$$

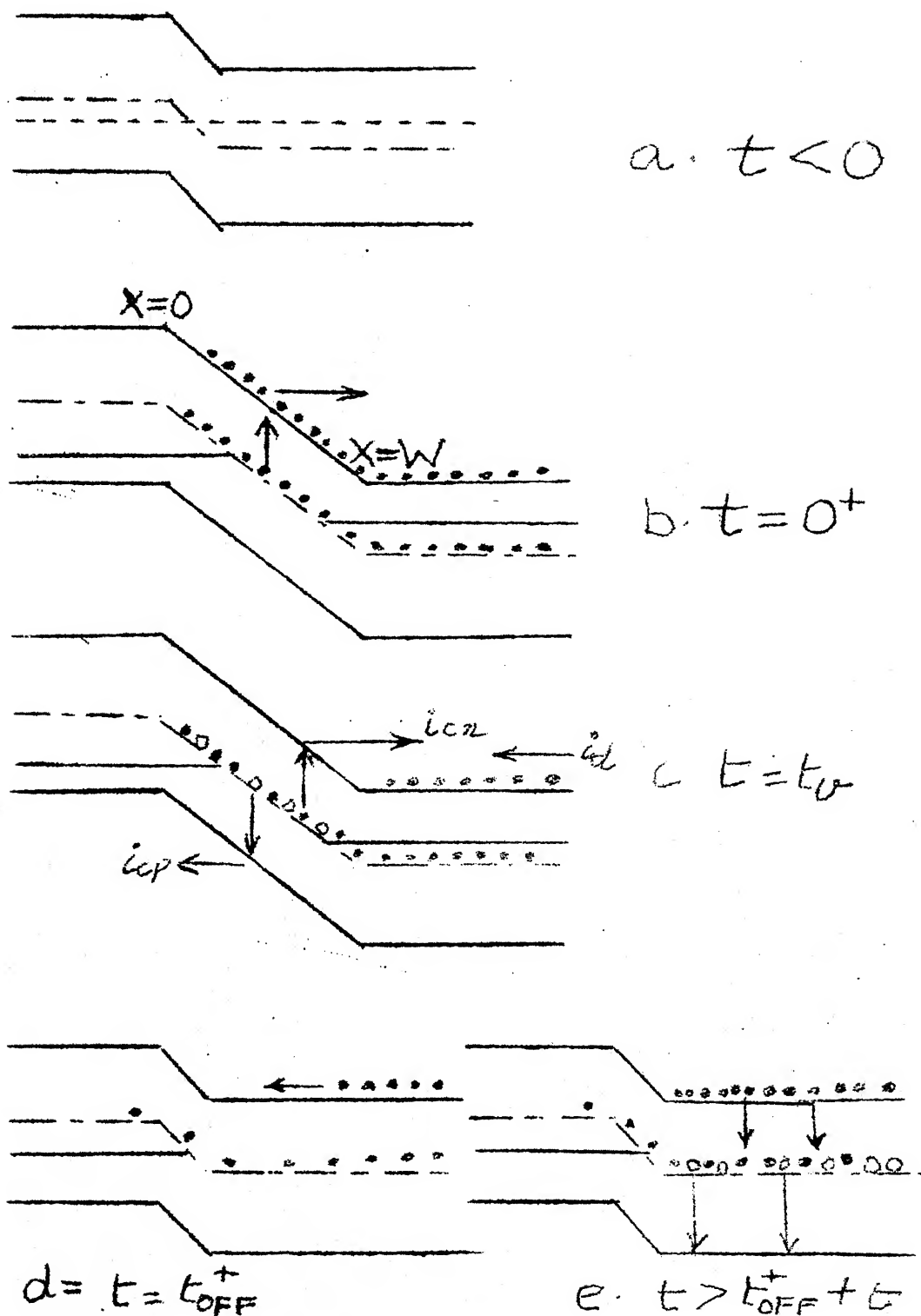$$= \frac{qwA}{2} \left(\frac{dn_T}{dt}\right) \qquad (2.21)$$

Fig. 2.3: Energy band diagram during the switching transients

Combining eqn. (2.20) and (2.21) and ignoring conduction current due to holes, which will be small in n-type semiconductor:

$$i = i_{c_n} + i_d = \frac{qWA}{2} (e_p p_T + e_n n_T) \tag{2.22}$$

and for case of $p^+N$ junction (2.22) becomes

$$i = \frac{qWA}{2} e_n n_T \tag{2.23}$$

For an acceptor level (2.23) becomes

$$i = \frac{qWA}{2} e_n N_{TT} e^{-t/z_n} \tag{2.24}$$

using the expression for W in (2.15) and (2.24) becomes

$$i = \frac{qW_\infty A e_n N_{TT}}{2} \left[ 1 - \frac{N_{TT}}{N_D} e^{-t/z_n} \right]^{-1/2} e^{-t/z_n} \tag{2.25}$$

where,

$$W_\infty = \left[ \frac{2 \mathcal{E} V_i}{q N_D} \right]^{1/2}$$

If $N_{TT} \ll N_D$, (2.25) becomes:

$$i = \frac{qA e_n N_{TT}}{2} W_\infty e^{-t/z_n} \tag{2.26}$$

Hence the current transient is exponential when $N_{TT} \ll N_D$, otherwise it is nonexponential.

The timing diagram for both current and capacitance transient in case of majority carrier pulse is shown in Fig. 2.4.

## 2.3 TECHNIQUES USED IN ANALYSIS OF TRANSIENTS:

This section briefly discusses the various techniques used to get trap data. They are essentially of two types called single shot methods and synchronous detection methods. In both the aim is to get Arrhenius plot.

### 2.3.1 Single Shot Methods:

They were historically the first methods to be used for analysis and are accurate but are very painstaking. Prime examples of this in our case are conventional iso- thermal capacitance transient study and isothermal current transient study [4]. Herein the time constants of transients are found and each point in Arrhenin's plot is obtained thereby.

### 2.3.2 Concept of DLTS:

Deep Level Transient spectroscopy is a synchronous detection method. It has been used very extensively in getting trap parameters. The major feature of this method is that it is fast, sensitive and spectroscopic in nature [5]. A wide variety of traps can be detected by observing
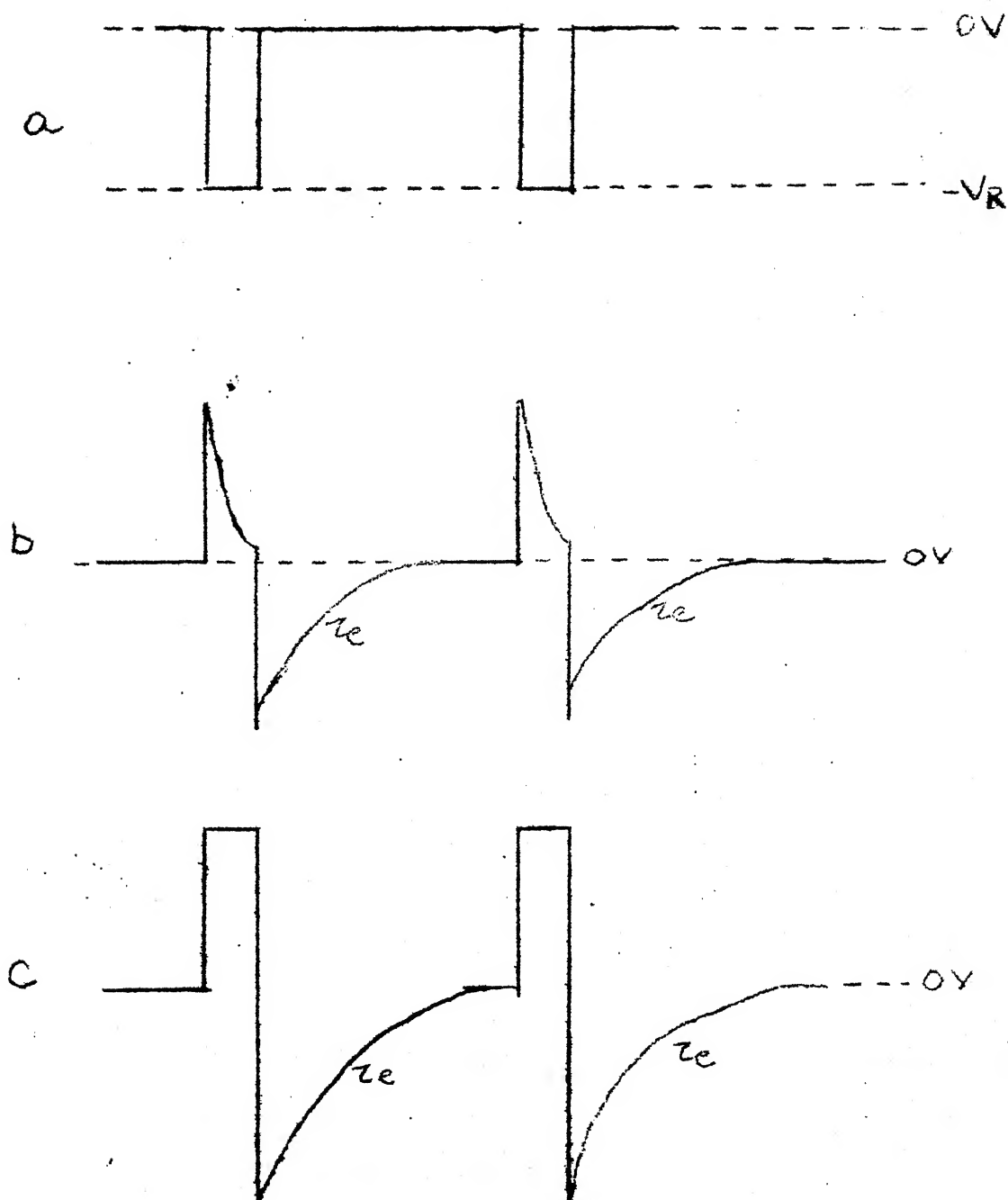
Fig. 2.4: Timing diagram of
b) current transients and c) capacitance transients corresponding to majority carrier pulse in (a).

the DLTS spectrum. The essential feature of DLTS is that one can set a rate window in a Box-car integrator as depicted in Fig. 2.5. The difference signal $C(t_1)-C(t_2)$ or $i(t_1)-i(t_2)$ is plotted as a function of temperature. The sign of the trap tells whether it is an electron or a hole trap and temperature corresponding to maximum gives one point on the Arrhenius plot. The value of $e_n$(or $e_p$) needed can be related to difference $(t_1-t_2)$ through following:

Normalised DLTS signal is given by

$$= [C(t_1) - C(t_2)]/\Delta C(o)$$

where $C(o)$ is the capacitance change at $t = o$.

For exponential transients

$$S(t) = [\ e^{-t_1/\tau} - e^{-t_2/\tau}\ ] \qquad (2.27)$$

where $\tau$ is the time constant of the transient.

Maximising eqn. (2.27) with respect to by differentiating and equating it to zero gives

$$\tau_{max} = (t_1-t_2)\ [\ln [t_1/t_2]] \qquad (2.28)$$

Thus one needs simply to scan the temperature and observe the DLTS spectra for each scan. The sign of peaks and position of peaks need to be observed and from this and
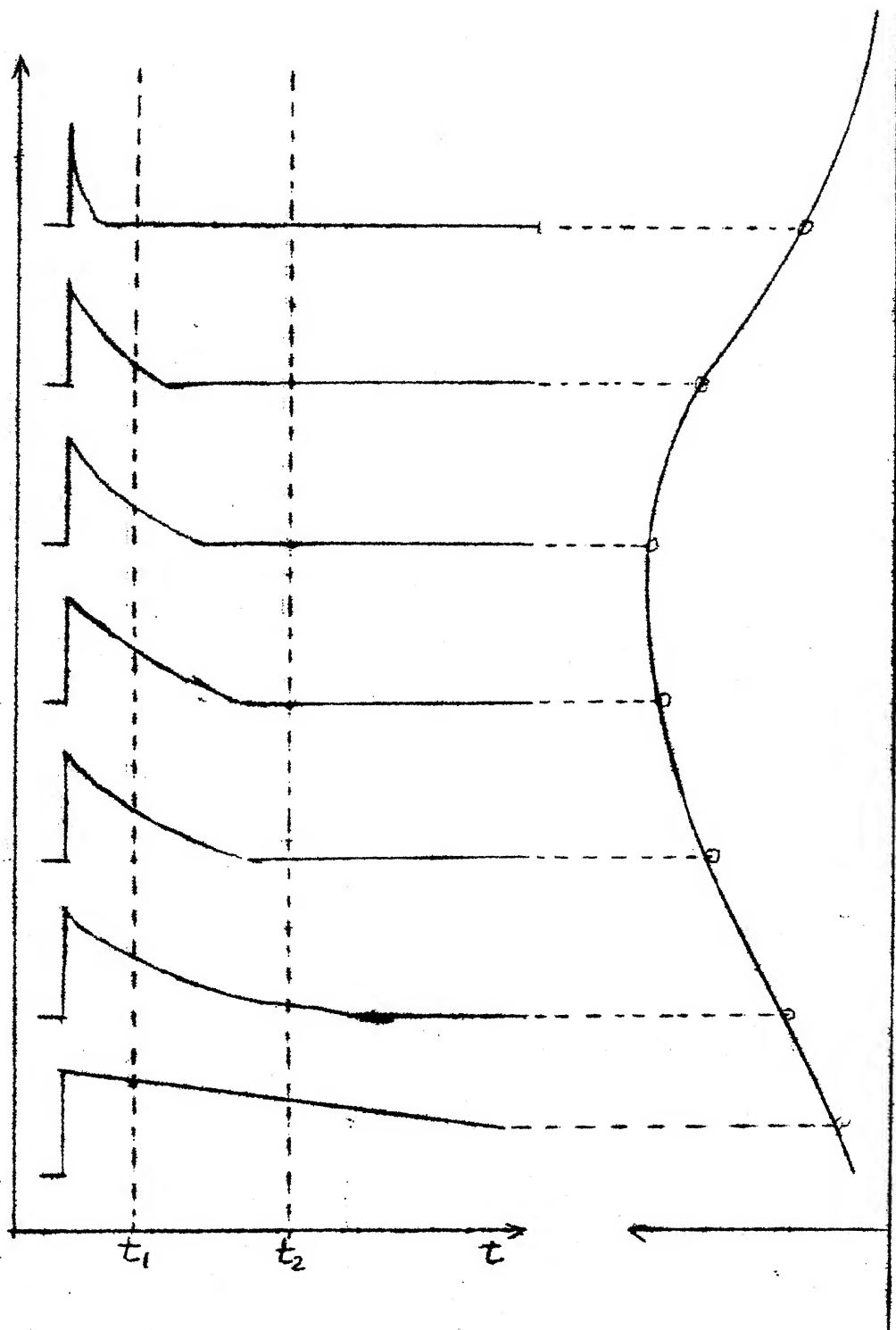
Fig. 2.5: Rate windowing concept.

values of $t_1$ and $t_2$ using eqn. (2.28), one can get an
Arrhenins plot. Some remarks are in order:

1. This method is applicable to exponential transients
only as evident from eqn. (2.27). Any non-adherence to
this criterion will give wrong values for activation energy,
capcture cross-section and related parameters [7]. It has
been further found that choice of $t_1$ and $t_2$ can give widely
different Arrheni s plots in such cases.

2. Even for a single exponential, the conventional
DLTS uses inefficiently the data, it gets in each scan.
Hence modifications have been suggested [8] where the rate
windowing concept is done in software after recording all
the transients in a single scan.

3. DLTS subtracts the offset due to leakage current
or steady state capacitance and thus overcomes a serious
problem affecting the single shot analyses.

4. Finally DLTS is at best a very good survey technique
and can in no way supplant careful and accurate
determination possible through single shot analysis.

CHAPTER 3

TRANSIENT DATA ANALYSIS

## 3.1 INTRODUCTION:

The isothermal relaxation data is characterized
by two major factors:

a) That the transients sit on a steady state level
$\triangle I_o$ or $\triangle C_o$, leading to the form $Ae^{-\alpha t} + B$.

b) That in the presence of multiple traps, the data
has multiexponential decay of the form $\sum_{i=1}^{n} A_i e^{-\alpha_i t}$.

At the outset, one might feel that determination of
the values of $A_i$ and $\alpha_i$ in the above is a trivial problem.
However, it is not so [11]. Even for a single exponential
case in (a) above to get an accurate and reliable value for
A, $\alpha$ and B is a difficult exercise. In this chapter these
aspects of the problems have been studied.

## 3.2 ANALYSIS FOR SINGLE EXPONENTIAL:

Initially the problem of determination of decay
constant in single-exponential transient seems very easy.
One can think of simply finding the ratio of the transient
curve at two values and computing the decay constant. Or
one could fit the logarithm of the transient curve to a

straight line using linear regression algorithm, thereby getting both A and $\alpha$. However the offset B frustrates any such simple implementation. Hence the aim is to somehow remove this B and use the conventional methods thereafter or devise a suitable algorithm which takes B into account. The problem is further exacerbated by certain limitations of the signal analyser, detailed later on in the chapter. In any case, one has to be careful. Several methods have been suggested to remove this B accurately. Particularly in case of isothermal relaxation two ways were found to determine the value of B:

a) One uses the physical origin of this constant offset. In either current or capacitance transients, $\Delta I_o$ or $\Delta C_o$ emanate from the leakage current or steady state junction capacitance during the time of reverse bias in both minority carrier and majority carrier pulses. Hence for a given device, one can reverse bias it to the same conditions as that of pulses and obtain values of $\Delta I_o$ and $\Delta C_o$. However the major problem in this lies in obtaining identical conditions repeatedly for each temperature. Hence it is not a very attractive method.

b) The other method to determine B, is to take average of a number of points on the tail of the transient and then subtract this average value from the whole curve.

However, scatter due to noise in the signal precludes dependence on only a few points. Hence one needs to take a large enough number of points on the tial portion so that randomness of noise cancels and helps in accurate determination of B. Such requirement, particularly, in case of low temperature slow transients is not readily possible.

One can then think of logical extension of the basic methods. One such extension is:

## 3.2.1 Ratio Method:

Herein we take three points on the transient and solve the resulting transcendental equation. Its brief description is as follows:

Three points on the transient curve $Ae^{-\alpha t} + B$ are:

$$Y_1 = Ae^{-\alpha t_1} + B \tag{3.1}$$

$$Y_2 = Ae^{-\alpha t_2} + B \tag{3.2}$$

$$Y_3 = Ae^{-\alpha t_3} + B \tag{3.3}$$

From eqns. (3.1), (3.2) and (3.3), we get

$$Y_2 - Y_1 = A(e^{-\alpha t_2} - e^{-\alpha t_1}) \tag{3.4}$$

$$Y_3 - Y_2 = A(e^{-\alpha t_3} - e^{-\alpha t_2}) \tag{3.5}$$

Using eqn. (3.4) and eqn. (3.5), one gets

$$\frac{y_2 - y_1}{y_3 - y_2} = \frac{e^{-\alpha t_2} - e^{-\alpha t_1}}{e^{-\alpha t_3} - e^{-\alpha t_2}} \tag{3.6}$$

Values of $y_1, y_2, y_3$, $t_1, t_2$ and $t_3$ are known from the transient data and one has to solve this transcendental equation. Using Newton-Raphson method, one can solve this iteratively. Normally one should get a reliable and satisfactory result. However numerical snags come up, when evaluating it. This is because even slight variations in the values of $t_1$, $t_2$ or $t_3$ gives widely varying values of $\alpha_i$'s. Actually this is symptomatic of all problems dealing with exponentials. This method, therefore, demands very accurate measurements of $t_1$, $t_2$ and $t_3$. Table 3.1 emphasizes the above contention. An alternative method is, hence thought of:

## 3.3.2 Area Method:

Here transient with a positive d.c. shift is assumed, though for negative offsets too, the same procedure holds. A (current) transient from the relaxation process with a positive offset is shown in Fig. 3.1.

The three equations in this case are:

$$X_1 = A + B \tag{3.7}$$

Table 3.1: Results from ratio method analysis

| $t_0$ in μs | $t_1$ in μs | $t_2$ in μs | $t_3$ in μs | A | α | B |
|---|---|---|---|---|---|---|
| 0 | 0 | 0 | 0 | 0.285603 | 13610.6 | 0.226716 |
| +2β | X | X | X | 0.267275 | 13621.6 | 0.22678 |
| +2β | X | X | X | 0.233989 | 13631.7 | 0.226838 |
| −2β | X | X | X | 0.305109 | 13592.2 | 0.226608 |
| −6β | X | X | X | 0.348874 | 13633.9 | 0.226851 |
| 0 | +2β | 0 | 0 | 0.281506 | 12557.3 | 0.220042 |
| 0 | +4β | 0 | 0 | 0.279169 | 10867.5 | 0.206545 |
| 0 | +6β | 0 | 0 | 0.312894 | 6533.76 | 0.139164 |
| 0 | −2β | 0 | 0 | 0.287909 | 14063 | 0.229265 |
| 0 | −4β | 0 | 0 | 0.295239 | 15257 | 0.235239 |
| 0 | −6β | 0 | 0 | 0.292871 | 14884 | 0.233479 |
| 0 | −10β | 0 | 0 | 0.300032 | 15863 | 0.237912 |
| 0 | 0 | +2β | 0 | 0.291945 | 16529.6 | 0.242591 |
| 0 | 0 | +4β | 0 | 0.290297 | 16061.2 | 0.240467 |
| 0 | 0 | +6β | 0 | 0.287189 | 14965 | 0.234946 |
| 0 | 0 | +10β | 0 | 0.292163 | 10658.4 | 0.200881 |
| 0 | 0 | −4β | 0 | 0.297631 | 17829.1 | 0.24783 |
| 0 | 0 | −6β | 0 | 0.295431 | 17367.7 | 0.246071 |
| 0 | 0 | 0 | +4β | 0.285849 | 13564 | 0.226259 |
| 0 | 0 | 0 | +6β | 0.290505 | 12782.7 | 0.218111 |
| 0 | 0 | 0 | +10β | 0.28221 | 14338.3 | 0.233456 |
| 0 | 0 | 0 | −4β | 0.291403 | 126505 | 0.216632 |
| 0 | 0 | 0 | −6β | 0.293571 | 12349.9 | 0.213153 |
| 0 | 0 | 0 | −15β | 0.349857 | 8266.78 | 0.1405 |
| 0 | +2β | +4β | +10β | 0.287851 | 15939.9 | 0.240383 |
| 0 | −10β | −15β | +10β | 0.299729 | 17945.7 | 0.246896 |
| +3β | +5β | −7β | +2+ | 0.259482 | 16174.4 | 0.239715 |
| −2β | −5β | +4β | +9β | 0.319644 | 16026.8 | 0.238732 |

$t_1$ = 43.9451 μs, $t_2$=68.359 μs, $t_3$=117.187 μs, $t_0$ = 0
β = 2.4414 μs, X = Corresponding change, $t_1, t_2$ etc −
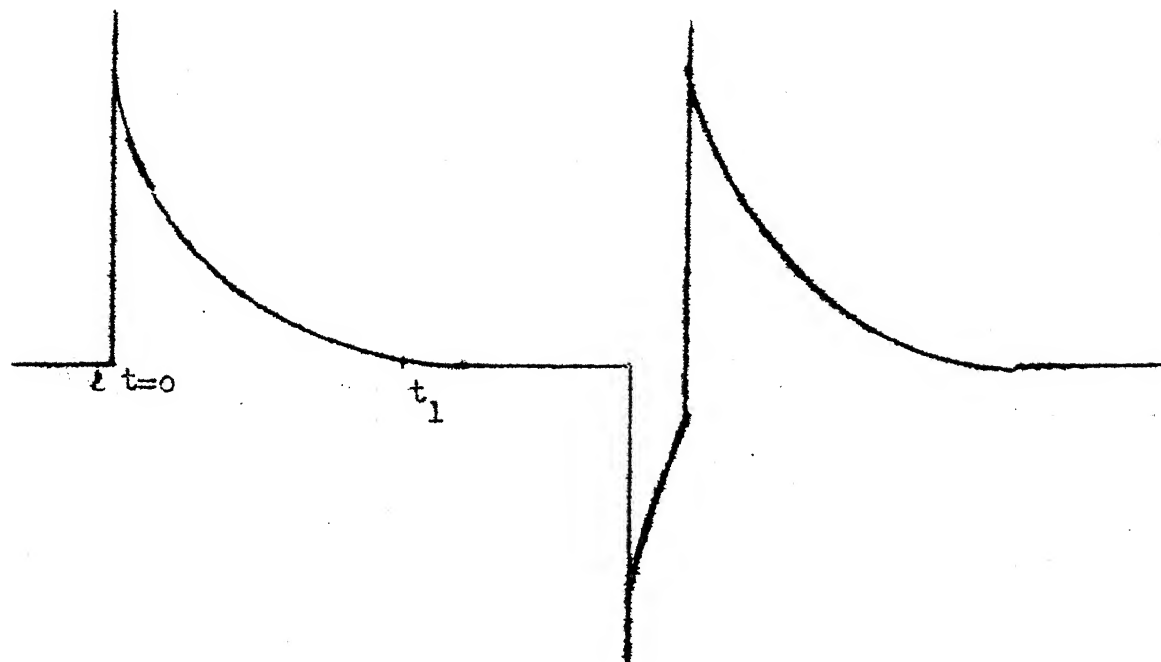changes in $t_1, t_2$ etc.

Fig. 3.1: A typical (current) transient.

$$X_2 = Ae^{-\alpha t_1} + B \qquad (3.8)$$

and

$$K = \int_0^{t_1} (Ae^{-\alpha t_1} + B) \, dt \qquad (3.9)$$

eqn. (3.9) on evaluation, gives

$$K\alpha = A[1-e^{-\alpha t_1}] + B\alpha t_1 \qquad (3.10)$$

Using $B = X_1 - A$ from eqn . (3.7) in eqn. (3.8) we get for A,

$$A = \frac{X_1 - X_2}{(1-e^{-\alpha t_1})} \qquad (3.11)$$

Substituting eqn. (3.11) in eqn. (3.10), we get:

$$(X_1-X_2)[1-\alpha t_1 - e^{-\alpha t}] = (1-e^{-\alpha t_1}) (K-X_1 t_1)\alpha$$
$$(3.12)$$

The above transcendental equation can be solved by observing the zero cross-over, for monotonically increasing $\alpha$.

The values of $\alpha$, $\blacksquare$ $\blacksquare$ $B$ obtained from this method have been found to be accurate and less susceptible to initial data variations than the Ratio method. Table 3.2 illustrates the above point. It further shows that the variation in $\alpha$ value with different choices of $t_o$ ($t=o$) is not acceptable. Unfortunately an accurate determination of $t_o$ is not easily possible for current transients. This is precisely due to two factors:

## Table 3.2

### Results from Area Method

| $t_0$ | $t_1$ | $\alpha$ | B |
|---|---|---|---|
| 0 | 0 | 12825 | 0.216796 |
| $+2\beta$ | 0 | 9775 | 0.216796 |
| $+6\beta$ | 0 | 9675 | 0.216796 |
| $-2\beta$ | 0 | 13825 | 0.216796 |
| $-4\beta$ | 0 | 9525 | 0.216796 |
| 0 | $+2\beta$ | 13550 | 0.217285 |
| 0 | $-2\beta$ | 14550 | 0.217285 |
| 0 | $-4\beta$ | 14225 | 0.218261 |
| 0 | $-6\beta$ | 16025 | 0.219726 |
| $+2\beta$ | $-2\beta$ | 10100 | 0.219726 |
| $-3\beta$ | $-4\beta$ | 10000 | 0.218261 |
| $-\beta$ | $+\beta$ | 9500 | 0.217285 |

$t_0 = 0$, $t_1 = 2.13378$ ms, $\beta = 2.4414$ µs

$t_0, t_1$ — changes in $t_0$ and $t_1$ respectively.

a) 100 KHz bandwidth of the signal analyser and hence existence of reasonably strong Gibb's effect.

b) A large current component due to sweep-out of majority carriers in the sample, saturates the current transient measurement set-up.

The cumulative effect of both is that accurate $t_0$ determination is not possible. However the redeeming feature of the area method, as from Table 3.2, is that the variations in B, due to fluctuations in choice of $t_0$ instant are very small. Therefore our analysis for single exponential transients with offset, starts with Area method, where from the value of B is determined. This B is subtracted from the total curve and conventional methods are applied to get the values of A and $\alpha$ accurately.

The above analysis proceeds on the assumption that a single exponential decay is present. What if it is not so, as it is in the case of multiple traps where we may force unknowingly a multiexponential of the form $\sum\limits_{i=1}^{n} A_i e^{-\alpha_i t}$ to a single exponential. According to Lanczos [11], satisfaction of equivalence of the measured results to the computed ones using either one or more decay constants is no indicator of the actual values. For example the data in Table 3.3 for a double exponential signal can be, within

34

Table 3.3: Illustration of numerical equivalence of two different exponential expressions.

| t in microseconds | Actual double exponential $1e^{-5000t}+2e^{-10000t}$ | Least square single exponential $2.98375e^{-8056.71t}$ |
|---|---|---|
| 0 | 2.99988 | 2.98372 |
| 2.4414 | 2.93957 | 2.92562 |
| 4.8828 | 2.88049 | 2.86863 |
| 7.32418 | 2.82275 | 2.81276 |
| 9.76558 | 2.76623 | 2.75797 |
| 12.2069 | 2.71094 | 2.70426 |
| 17.0897 | 2.60388 | 2.59994 |
| 21.9725 | 2.50134 | 2.49964 |
| 24.4139 | 2.45178 | 2.45096 |
| 26.8553 | 2.4032 | 2.40322 |
| 34.1795 | 2.26379 | 2.26551 |
| 39.0623 | 2.17579 | 2.17811 |
| 43.9451 | 2.09155 | 2.09412 |
| 51.2693 | 1.97168 | 1.97416 |
| 56.152 | 1.896 | 1.89804 |
| 63.4762 | 1.78845 | 1.78937 |
| 70.8004 | 1.68701 | 1.68697 |
| 80.5659 | 1.56201 | 1.55961 |
| 85.4428 | 1.5033 | 1.49966 |
| 90.3315 | 1.44702 | 1.44109 |
| 95.2144 | 1.39307 | 1.3855 |
| 100.097 | 1.34131 | 1.33205 |

Least mean square error for 300 points = $.151819 \times 10^{-2}$

the accuracy of measurements, fitted to a single exponential. Comparing the two data lists one finds that error indeed is very small. In order to be more confident in case of single exponential analysis as well as to ascertain the existence of multiple traps, it is mandatory to know values of n, $A_i$ and $\alpha_i$ in $\sum_{i=1}^{n} A_i e^{-\alpha_i t}$. This is dealt in next section.

## 3.3 ANALYSIS FOR MULTIEXPONENTIAL SIGNALS:

Several methods are known for this important analysis According to Lanczos [11], it is not the limitation of the methods of analysis, which gives us unsatisfactory results but that the accuracy of initial data is not good enough to take care of extreme sensitivity of exponentials to scatter in initial data. Hence a method due to Gardner et.al. [12] is described. In this method the end result is in the form of peaks corresponding to each of the exponents in the multiexponential signal. This method is subdivided into three main subsections viz. theory, implementation ~~and~~ & results and application to relaxation data.

### 3.3.1 Theory:

We are given the function $f(t) = \sum_{i=1}^{n} A_i e^{-\alpha_i t}$ and we wish to determine n, A and $\alpha_i$. The above Dirichlet series is converted to Stieltjes integral:

$$f(t) = \sum_{i=1}^{n} A_i \, e^{-\alpha_i t} = \int_{0}^{\infty} e^{-\alpha t} \, dh(\alpha) \qquad (3.13)$$

where $h(\alpha)$ is a sum of step functions. Eqn. (3.13) can be expressed in terms of Delta functions as:

$$f(t) = \int_{0}^{\infty} e^{-\alpha t} \, g(\alpha) \, d\alpha \qquad (3.14)$$

The quantity $g(\alpha)$ contains information about the various $\alpha_i$ values. The aim is hence to solve for $g(\alpha)$. The solution of this integral equation is done by transforming the variables $\alpha$ and $t$ as $\alpha = e^{-y}$ and $t = e^{x}$.

Then eqn. (3.14) becomes

$$f(e^{x}) = \int_{-\infty}^{\infty} \exp[e^{-(x-y)}] g[e^{-y}] e^{-y} dy \qquad (3.15)$$

comparing eqn. (3.14) and (3.15), one finds

$$g(\alpha) d\alpha = \alpha g(e^{-y}) dy$$

or

$$\left(\frac{g(\alpha)}{\alpha}\right) d\alpha = g(e^{-y}) dy \qquad (3.16)$$

Hence a plot of $g(e^{-y})$ with respect to $y$ is equivalent to plot of $g(\alpha)$ with respect to $\alpha$. Therefore we need to find ways to get $g(e^{-y})$ from eqn. (3.17). We multiply eqn. (3.15) by $t = e^{x}$, then eqn. (3.15) becomes:

$$e^X f(e^X) = \int_{-\infty}^{\infty} \exp[-e^{X-Y}] \ e^{X-Y} \ g(e^{-Y}) dy \qquad (3.18)$$

We define Fourier transform $F(\mu)$ as

$$F(\mu) = \frac{1}{\sqrt{2\pi}} \int_{-\infty}^{\infty} e^X f(e^X) e^{i\mu x} \ dx \qquad (3.19)$$

Hence eqn. (3.18) becomes using eqn. (3.19),

$$F(\mu) = \frac{1}{\sqrt{2\pi}} \int_{-\infty}^{\infty} \int_{-\infty}^{\infty} \exp[-e^{X-Y}] \ e^{X-Y} g(e^{-Y}) dy \ \exp(i\mu x) dx$$

$$(3.20)$$

Putting $s = x-y$ and $x = s+y$ in eqn. (3.20) one gets:

$$F(\mu) = \frac{1}{\sqrt{2\pi}} \int_{-\infty}^{\infty} \int_{-\infty}^{\infty} \exp[-e^S] \ e^S \ g(e^{-Y}) dy$$

$$\exp(i\mu(s+y)) ds \qquad (3.21)$$

or eqn. (3.21) becomes

$$F(\mu) = \frac{1}{\sqrt{2\pi}} \int_{-\infty}^{\infty} g(e^{-Y}) \ \exp(i\mu y \ dy \int_{-\infty}^{\infty} \exp(-e^S) e^S$$

$$\exp(i\mu s) ds \qquad (3.22)$$

In eqn. (3.22), one finds that first integral can be called Fourier Transform $G(\mu)$ of $g(e^{-Y})$, while the second integral needs to be found separately. However the second integral

can be related to Euler integral of complex Gamma function, which is given by:

$$\Gamma(z) = \int_{-\infty}^{\infty} e^{-t} \, t^{z-1} \quad \text{for} \quad > o \qquad (3.23)$$

Substituting $t = e^{s}$ in eqn. (3.23) one gets

$$\Gamma(z) = \int_{-\infty}^{\infty} \exp(-e^{s}) \, e^{s(z-1)} \, e^{s} \, ds \qquad (3.24)$$

If $z = 1+i\mu$, then

$$\Pi(1+i\mu) = \int_{-\infty}^{\infty} \exp(-e^{s}) \, e^{i\mu s} \, e^{s} \, ds \qquad (3.25)$$

This is what exactly is the second integral in eqn. (3.22). Fortunately values of Gamma function are available in tabulated form. Defining $K(\mu)$ as

$$K(\mu) = \frac{1}{\sqrt{2\pi}} \, \Gamma(1+i\mu)$$

one gets from eqn. (3.22),

$$F(\mu) = K(\mu) \cdot G(\mu)$$

or

$$G(\mu) = \frac{F(\mu)}{K(\mu)} \qquad (3.26)$$

If one takes the inverse Fourier transform of eqn. (3.26), then one gets

$$g(e^{-y}) = \int_{-\infty}^{\infty} G(\mu)\ e^{-i\mu y}\ d\mu \qquad (3.27)$$

Hence a plot of $g(e^{-y})$ with respect to y will give the value of exponents as peaks, the amplitudes of which are proportional to $N_i/\alpha_i$.

3.3.3 Implementation and Results:

The above algorithm is implemented using BASIC program on the signal analyser (IWATSU model SM2100B). The integrations are done by Simpson's method. The listing of the program is given in Appendix II. To prove the method, both analytical and experimental data were taken. Figs. 3.2 to 3.5 illustrate the results of the analysis. The analysis is in the form of a plot of $g(\alpha)$ as a function of $\alpha$. However such a plot cannot be directly obtained in the signal analyser, primarily because of the fact that a given function can be displayed only at discrete instants of time. The functional values at each of these instants are stored in the form of an array in the memory. These array locations are accessible through software. The above fact is exploited by storing $\alpha$ and $g(\alpha)$ values simultaneously in two different arrays. And when the two arrays are displayed, the values read by the cursor at each instant give the values of $g(\alpha)$ and $\alpha$.

To appreciate the multiexponential analysis, four examples in Figs. 3.2 to 3.5 are used to illustrate its various details:

1. All the plots in each figure show a spectra like behaviour. This is so because of finite cut offs for x and $\mu$ variables in eqn. (3.18) and eqn. (3.27). For instance eqn. (3.18) with finite cut offs for x and $\mu$ is given by:

$$F(\mu) = \frac{1}{\sqrt{2\pi}} \int_{-x_0}^{+x_0} e^x f(e^x) \exp(i\mu x) dx + E[x_0,\mu] \qquad (3.28)$$

The extra term above is an indicator of the error due to cut offs in x and $\mu$. This error manifests itself in eqn. (3.26) where $F(\mu)$ is divided by $K(\mu)$. As the values of $\mu$ are increased, the $K(\mu)$ values decrease very rapidly and a small error $E(x_0,\mu)$ in $F(\mu)$ gets amplified to large error peak. This can be seen in Figs. 3.2 to 3.4 where as $\mu$ is increased from $\mu=3$ to $\mu=5$ and then to $\mu=7$, the number of peaks increases. In Fig. 3.5, the same thing is observed for $\mu=2$, $\mu=4$ and $\mu=6$.

2. The existence of error peaks in these can lead to loss of peaks, corresponding to actual $\alpha_i$ values. However the redeeming feature of this method is that as one varies values of $\mu$, the error peaks shift their position while real peaks do not. This is shown in each of the figures and for each of the $\mu$'s by placing the cursor at the peak or peaks, which move very little.
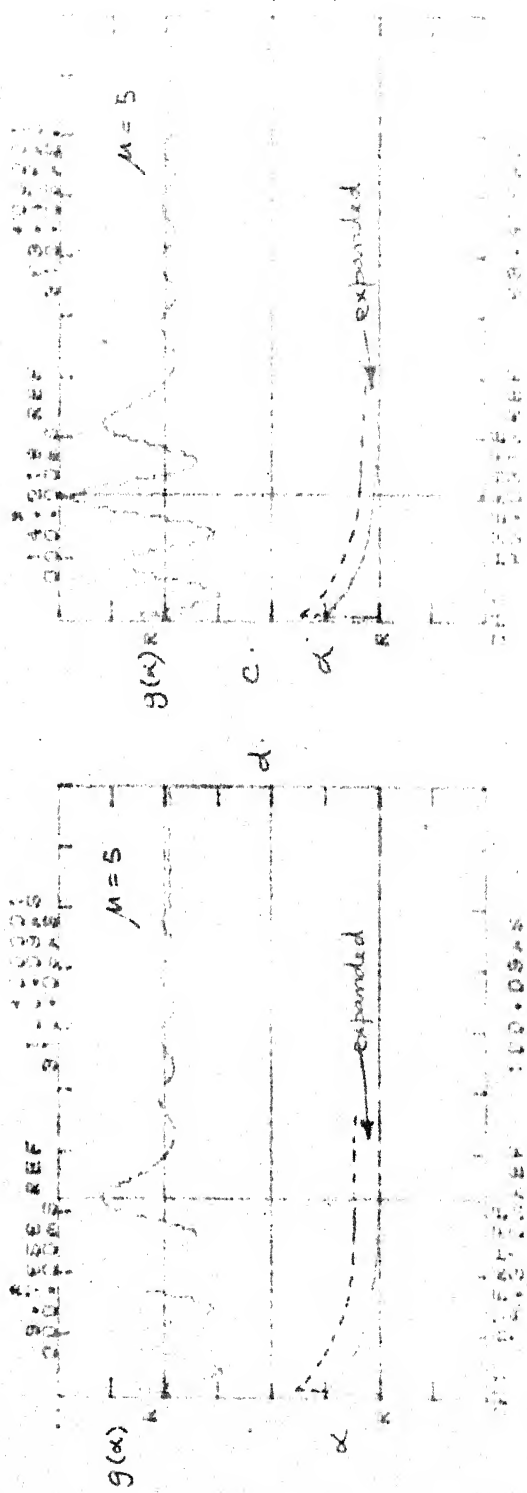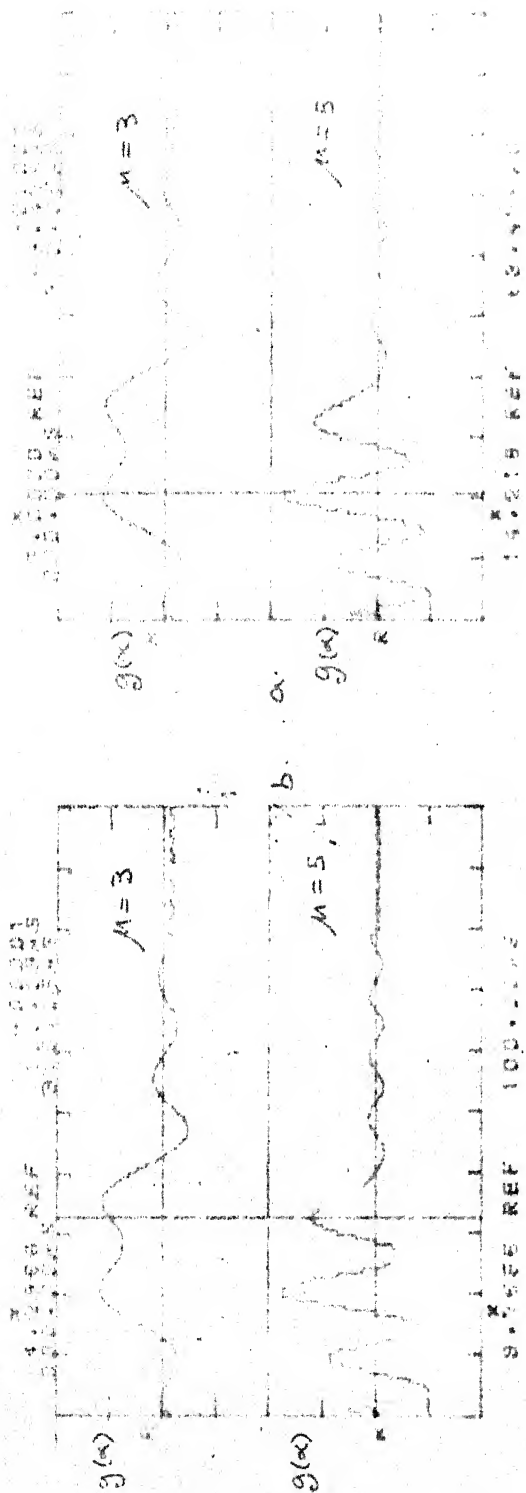
Fig. 3.3: Multiexponential analysis on analytically generated double
exponential $1e^{-16t} + 5 \cdot 1e^{-16t}$ (double exponential signal)
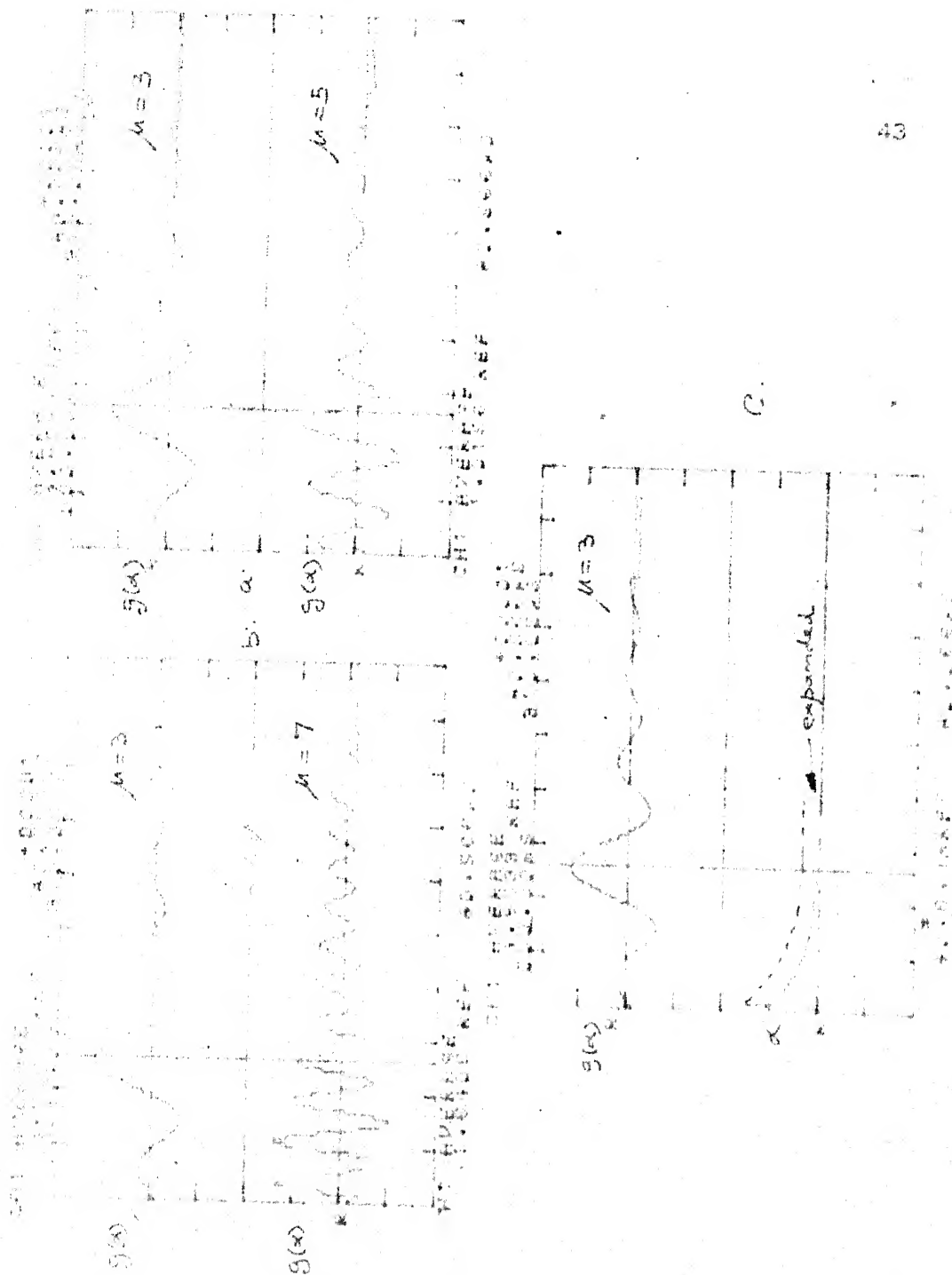
43

$M=3$

$M=5$

$g(x)$

$g(x)$

a.

b.

$M=3$

$M=7$

$g(x)$

$g(x)$

$M=3$

c.

$g(x)$

expanded

Fig. 24: Fourier-differential analysis on experimentally obtained $1.0 \cdot e^{-4000t}$
scaling factor $1.0 \cdot 10^{-4}$ and a value (s=m) $f(x,t,q)$

$g(\alpha)$

$\mu = 4$

$g(\alpha)$

$\mu = 2$

$g(\alpha)$

$\mu = 6$

b.

a.

$g(\alpha)$

$\mu = 4$

CHI EXPER./PER.

CHI EXPER./PER.

CHI EXPER./PER.

$g(\alpha)$

$\mu = 6$

$g(\alpha)$

$\mu = 6$

expanded

expanded

$\alpha$

$\alpha$

$x$   165.09446F   927.73.
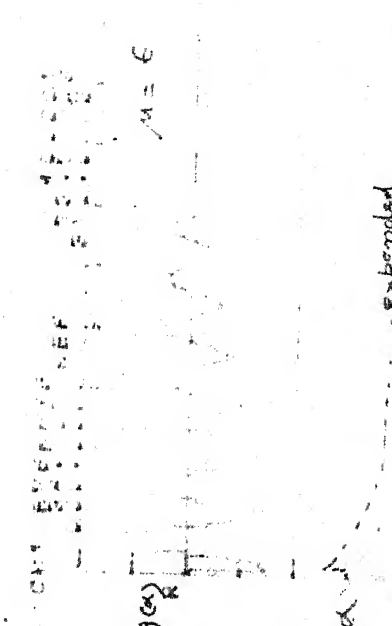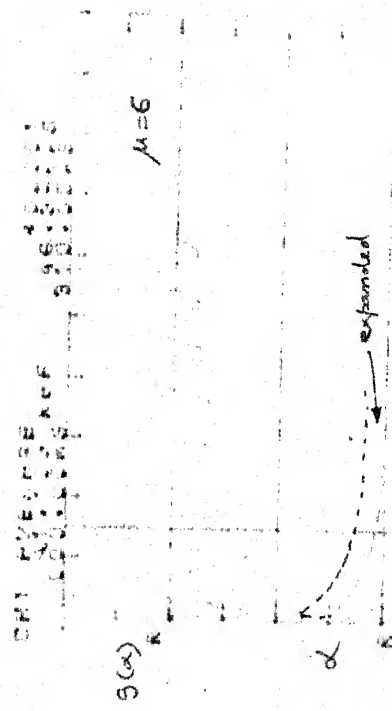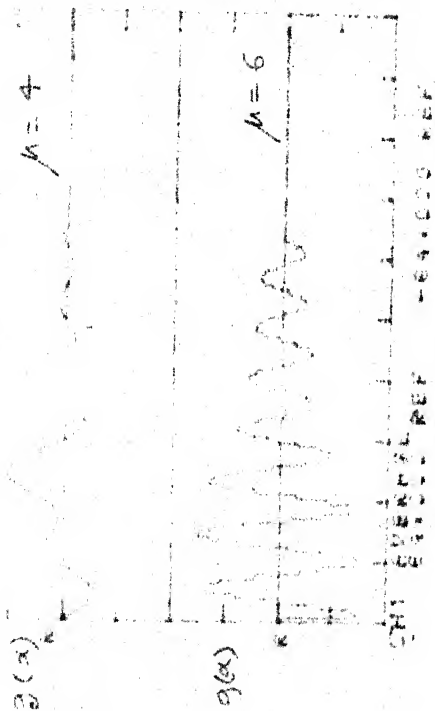
FIG. 3.5   Multiexponential analysis on experimentally obtained $1e^{-500ct} + 2 e^{-\ldots ct}$.
Scaling factor: 100000 , values found for $\alpha i$'s : 5493 F16525

3. The resolution of each actual peak is maximum at higher $\mu$'s and hence accurate $\mu_i$'s can be known by increasing $\mu$'s gradually so that these are properly distinguished at lower $\mu$'s when error peaks are smallest and accurately known at higher $\mu$'s, where their resolution is maximum.

4. The variation in $\alpha$ in all figures 3.2 to 3.5 is from 0 to 1. Hence all decay constants need to be scaled in time so that $\alpha$ falls between 0 and 1. For instance in Fig. 3.4 an exponential of the form $100e^{-4000t}$ is used. For decay constant to fall between 0 and 1, it is scaled in time as $100e^{-.04 \times (100000t)}$. The result of the analysis then would give the peak of $g(\alpha)$ at $\alpha = .04$. The value as read from Fig. 3.4(c) shows this $\alpha$ value as .040649. Similarly scaling is done in Fig. 3.5. In both the figures hence the scaling factor used is 100000. As the exponentials of Fig. 3.2 and 3.3 have exponents less than one, therefore no scaling is needed in these cases.

5. For the case where more than one exponent is present, $A_i$ should increase as $\alpha_i$ increases. For our illustration, the two double exponentials $1e^{-.016t} + 5e^{-0.8t}$ and $1e^{-5000t} + 2e^{-100000t}$ satisfy this condition.

6. Another precaution which needs to be taken is that the given exponential function should be properly sampled. If

the whole exponential information is not available as input to the algorithm, error is found in the determined $\alpha_i$ values. Fig. 3.6 shows how this particular effect in case of two different cut offs on the exponential gives a different $\alpha$ value. For the transient $100e^{-4000t}$, the values of $e^x f(e^x)$ are plotted in (a) and (b). The values along the abscissa are proportional to x values. In 3.6(a) the sampling is done till the exponential has totally decayed and in 3.6(b), the data obtained is only upto an earlier time instant, where the transient has not decayed completely. The results of the analysis show that for the case in 3.6(a), the peak occurs at 4064.9. This is seen in Fig. 3.6(c) while Fig. 3.6(d) shows $\alpha$ value as 5493.1 for abrupt cut off case.

7. Finally all the values found by multiexponential analysis in Figs. 3.2 to 3.5 are compared with the actual values. In Fig. 3.2, for analytical function $100e^{-.02t}$ the analysis is done at $\mu=3$, $\mu=5$ and $\mu=7$. Only one peak is seen to move very little along the abscissa. This peak is identified by the cursor and its value is read in (c) as .020141.

Fig. 3.3 analyses double analytic exponential $1e^{-.016t} + 5e^{-.08t}$. The $\mu$ value is varied from $\mu=3$ to $\mu=5$ to $\mu=7$. There are two peaks found to move very little and they are read in (c) and (d) as .018 and .082 respectively.
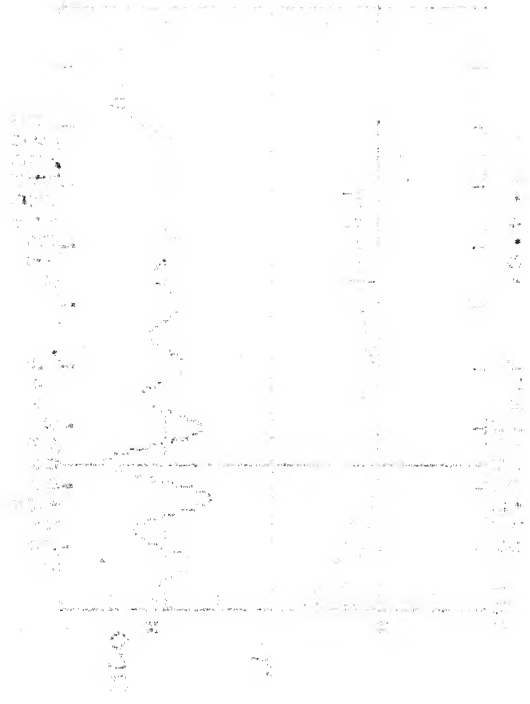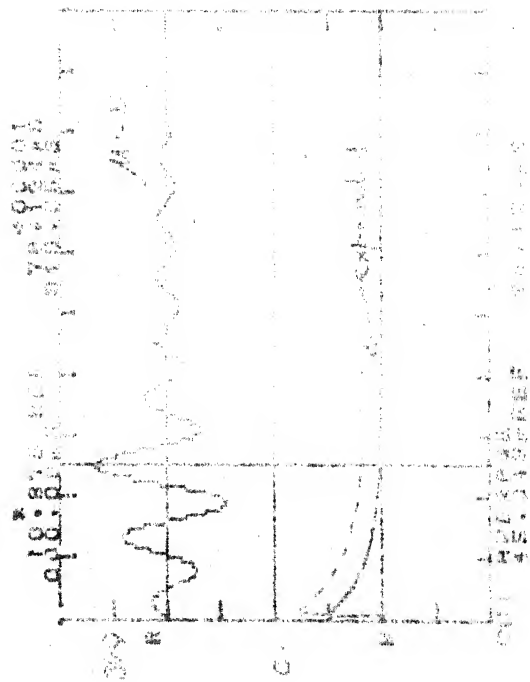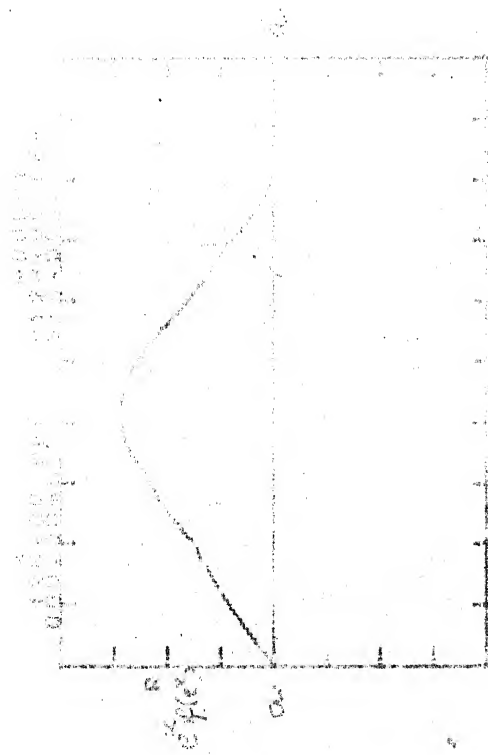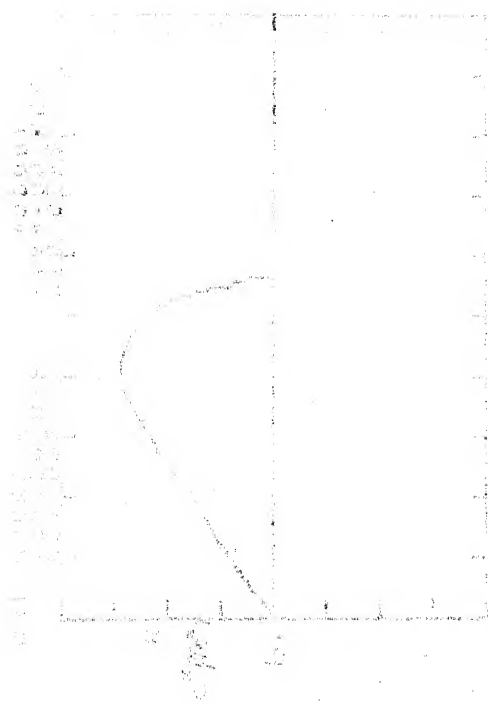
In Fig. 3.4 experimentally obtained single exponential is analysed at $\mu=3$, $\mu=5$ and $\mu=7$. One peak as identified by cursor is shown to be almost stationary. The value of $\alpha$ at this peak is read in (c) as .040642. As the scaling factor of 100000 was used, the actual $\alpha$ value is 4064.2.

Lastly the double exponent $1e^{-5000t}$ and $2e^{-1000t}$ in Fig. 3.5 is chosen particularly since it was found using conventional methods that this was numerically equivalent to its least square fitted expression $2.98375\ e^{-8056.71t}$ as shown in Table 3.3. Now as the multiexponential analysis is done on it, the two exponents show themselves clearly as $\mu$ is varied from 2 to 6 as shown in Fig. 3.5(a) and (b) respectively. At $\mu=2$ there is seen a broad peak, which breaks into two as $\mu$ is increased to 4 and then to 6. The values of $\alpha_i$'s at these peak points are read in Fig. 3.5(c) and (d) as .054931 and 1.6528. Using the fact that scaling factor of 100000 was used, the actual $\alpha_i$ values are 5493 and 16528.

Thus it is seen that multiexponential analysis is very convenient to detect multiexponents since the number and values of components fall out of the analysis. The following subsections discusses its application to relaxation data.

## 3.3.4 Application to Relaxation Data:

Application to particular case of isothermal relaxation is considered here. The following points can be made.

1. This method is used to ascertain the number of components in the transient and get their approximate values.

2. Because of the limitation listed in (6) in Section 3.3.3, the results from an unknown sample need to be considered carefully.

3. $\mu$ values need to be varied from the lowest possible to the largest possible values so that the true peaks are unambiguously distinguished.

4. Major problems faced when implementing the algorithm on the signal analyser are its long execution time and limited accuracy. Both limitations contribute to the determination of only approximate values, taken over relatively long times. Needless to say given a faster and more accurate machine, it is possible to get fairly accurate spectra.

## 3.4 ANALYSIS FOR DLTS:

DLTS, as explained in Chapter 2, is an elegant procedure for characterizing deep levels, even in the presence of multiple traps, which have reasonably apart activation energies. It has advantages over the above

analysis procedures, since it is spectroscopic in nature.
At the same time it retains the essential features of
space-charge relaxation methods. The conventional DLTS, as
mentioned in Chapter 2, uses inefficiently the data and
requires a double Box-car integrator. For each point in
Arrhenius plot, a separate thermal scan is needed. The time
and effort needed for this are prohibitive for very large
temperature variations. This disadvantage is overcome by
separating the acquisition of signal from its analysis [8].
In this modified procedure, the isothermal capacitance and
current are acquired and stored in memory of signal analyser.
Corresponding to setting of rate window in Box-car integrator,
a program is written, wherein variation of a single variable
changes the rate window. A DLTS spectrum is thus obtained.
However one should be careful in interpreting this data,
since now temperature is held constant and not varied
continuously.

# CHAPTER 4

## MEASUREMENT SYSTEM FOR DATA ACQUISITION

### 4.1 INTRODUCTION:

This chapter deals with the measurement aspects of capacitance and current transients. Both the signals have very low amplitude and hence are very noise prone. The capacitance measurement, particularly, has to be done at 500 KHz or above, since in order to monitor space charge capacitance, the monitoring signal should not disturb the transition capacitance. Section 4.2 deals with the measurement system used for data acquisition. Section 4.3 and 4.4 discuss, in particular, the design of capacitance and current measurement modules.

### 4.2 MEASUREMENT SYSTEM FOR DATA ACQUISITION:

The measurement system can be divided into four blocks, as shown in Fig. 4.1. A brief discussion is given for each block.

### 1. Cryostat:

This essentially contains a Liquid Nitrogen dewar and a sample holder to place the sample at various depths in the cryocan . The temperature variation can be done
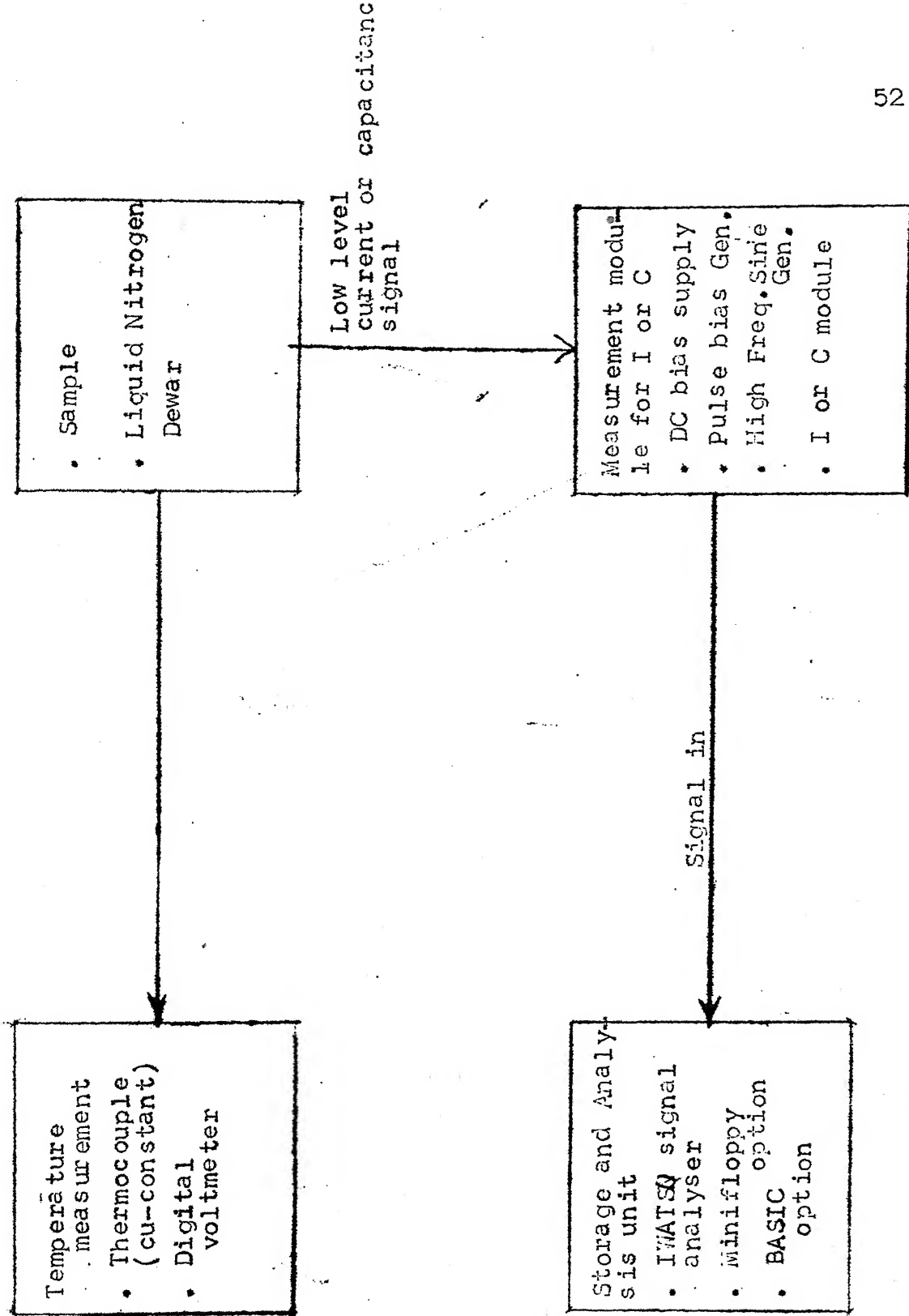
Fig. 4.1: Block diagram of measurement system for data acquisition.

exploiting the temperature gradient within the dewar. The temperatures above room temperatures can be obtained with the help of a soldering iron.

2. Temperature Measurement Block:

Temperature measurement is done with the help of a fine quality copper.- Constantan thermocouple. The thermocouple junction temperature is monitored directly with the help of a Digital multimeter (Keithley model 191). Room temperature correction is done after a mandatory warm up time of an hour or so. This is done by nulling this initial reading on the multimeter itself. An error of 2 to $3^{\circ}C$ can result in absence of this correction.

3. Signal Acquisition Block:

The acquisition block consists of following accessories, each of which is briefly described.

a) D.C. bias supply: This is needed in case of minority carrier pulse when the sample needs to be slightly forward biased. It is normally superimposed on the pulse bias.

b) Pulse bias supply: This is used to obtain the majority and minority carrier pulses. Here the pulse should be negative going from 0 V to -10 V. The pulse generator

used should have pulse rise and fall times of the orders of microseconds. In this case, Yamuna Pulse Generator has been used.

c) High frequency sinewave Generator: This is particularly used in case of capacitance transient measurements. The exact need for it is explained in the design of capacitance measurement module. The model used is GR-1210C.

d) Capacitance measurement module: This is used for getting both majority carrier and minority carrier trap transients. High frequency (500 KHz or more) sinewave is used to monitor the capacitance changes in the space charge region. Its design is explained later on in Sec.4.3.

e) Current measurement module: It is also used to get transients from majority and minority carrier traps. Its design details, too, are explained later on in Section 4.4.

4. Recording and analysis block:

These functions are performed by IWATSU signal analyser (model SM-2100B). The options necessary for our applications are:

a) Averaging: It is needed to improve the S/N ratio of very noisy capacitance and current transients from

the sample diode.  Summation averaging is used in this
case.

b) <u>Basic option:</u> This option is used to obtain the
various analys s programs described in chapter three.

c) <u>Minifloppy option</u>: This serves as our secondary
storage unit for the current and capacitance transients.
This helps in separating the acquisition from analysis, a
desirable  characteristic for DLTS.

4.3 DESIGN OF CAPACITANCE TRANSIENT MEASUREMENT MODULE:

The aim of this module is to measure the capacitance
change in the transition region of the sample, during the
relaxation process.  At the outset, one realizes that the
method used to measure capacitance should not disturb the
charge condition in the depletion region.  Hence the
monitoring signal should be both small in magnitude as well
as should be of high frequency such that charge change
should be slower than it.  Here this transient is measured
using principle of phase-sensitive detection.

4.3.1 Theory of Phase Sensitive Detection:

The principle of phase sensitive detection can be
explained using Fig. 4.2.

Here there are two channels  one is the reference
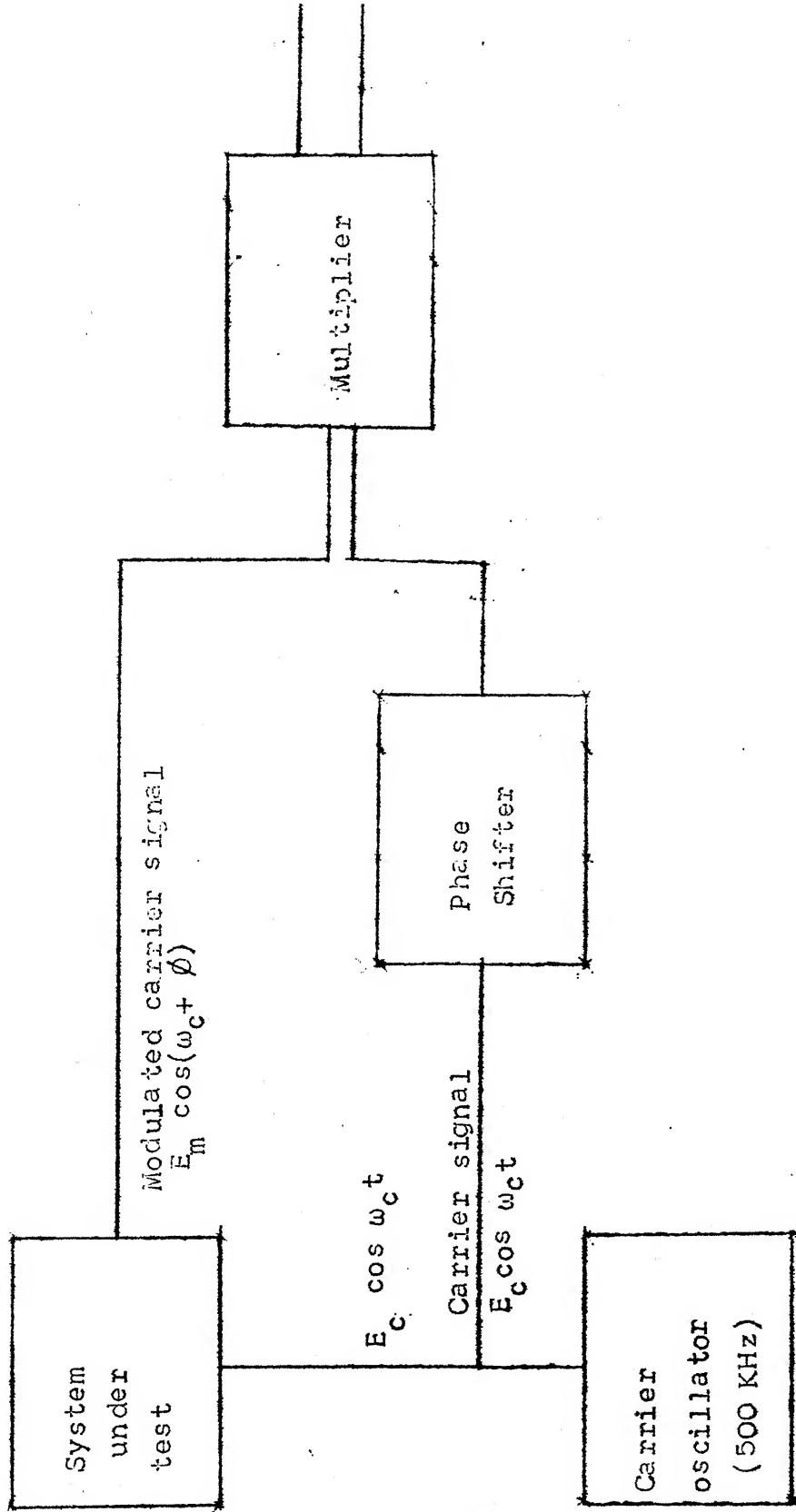channel and other is the channel through system under test.

Fig. 4.2: Block diagram of a phase sensitive detector

The diagram contains the following blocks and labels:

- System under test
- Carrier oscillator (500 KHz)
- Phase Shifter
- Multiplier

Signal labels:
- Modulated carrier signal $E_m \cos(\omega_c + \phi)$
- Carrier signal $E_c \cos \omega_c t$
- $E_c \cos \omega_c t$

Both the channels are locked-in to the same carrier signal frequency $\omega_c$. Hence the name lock-in detection also applies to the method. Calling the input signals to the multiplier as $X_1$ and $X_2$, then

$$X_1 = E_c \cos \omega_c t$$

$$X_2 = E_m \cos(\omega_c t + \phi)$$

Output $X_0$ of the multiplier will be $X_0 = X_1 X_2 = E_c E_m \cos \omega_c t \cdot \cos(\omega_c t + \phi)$.

$$X_0 = \frac{E_c E_m}{2} [\cos \phi + \cos (2\omega_c + \phi)] \qquad (4.1)$$

If we filter the output of the multiplier such that $\omega_{cutoff} \ll 2\omega_c$ then

$$X_0 = \frac{E_c E_m}{2} \cos \phi \qquad (4.2)$$

If in eqn. (4.2) now, a phase shifter is introduced in the reference channel such that phase difference between the two signals $X_1$ and $X_2$ is zero, then

$$X_0 = \frac{E_c E_m}{2} \qquad (4.3)$$

Hence if the 'system under test' is so designed that changes in capacitance are reflected as amplitude modulation of $E_m$, then $X_0$ the output signal will be proportional to capacitance

changes directly and we have succeeded in getting capacitance transients.

## 4.3.2 Design of Setup:

Keeping the above block diagram of Fig. 4.2 in mind, the capacitance measurement module should look like as in Fig. 4.3. A brief discussion of each block is given along with the realization.

a) <u>Summer</u>: Summer is needed to sum up three quantities:

1. Pulse bias 2. D.C. bias (for minority carrier pulse) 3. High frequency sinewave.

As operation needs to be done at high frequencies, LM318/CA3140 were found suitable for this application.

b) <u>I/V converter</u>: The design of this is the trickiest, since the signal level is quite low here and this being the first stage following Fritz's law, it needs to be as noise free as possible. It is instructive to know the order of currents available to be amplified by this converter.

Amplitude of carrier signal = 10 mV

Frequency of carrier signal = 500 KHz

Typical capacitance of 1N4148
diode (from data sheets) = 4 pF
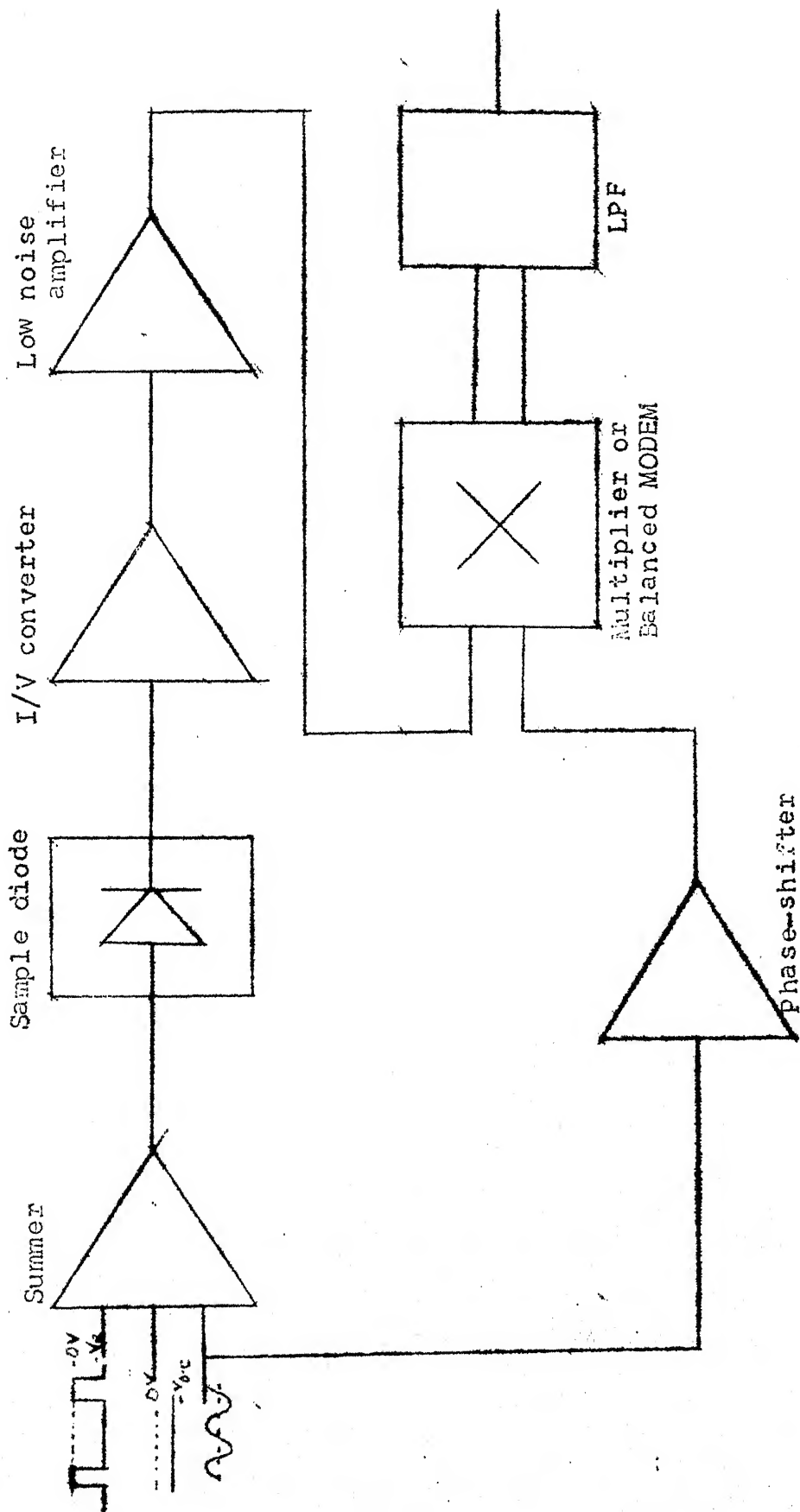
Fig. 4.3: Schematic of capacitance measurement module

Capacitive reactance of the diode

$$= \frac{1}{2\pi \times 500 \times 10^3 \times 4 \times 10^{-13}}$$

$$= 80K$$

Current through the diode $= \dfrac{10 \times 10^{-3}}{80 \times 10^3}$

$$= 100 \text{ nA}$$

This current has to be converted to voltage at 500 KHz and further amplified. The noise itself can be in millivolts and hence one needs to be careful. Here this is obtained by following steps:

a) This low current is dropped across a precision resistor. The value of this resistor is so chosen that it is much smaller than the impedance of diode in reverse bias and at that frequency.

b) The developed voltage is then buffered using a very low noise and excellent high frequency voltage follower LM310.

c) The buffered voltage is then amplified using a wideband amplifier (HP model 461A), having excellent input characteristics. However only gain of 10 is possible because amplifier oscillates due to mismatches at output.

d) The signal level still is low and hence the oscilloscope vertical amplifier output itself is taken. This output is applied to the multiplier block as one of its inputs.

C) <u>Phase shifter</u>: It is achieved using CA3140 in a phase-shifter configuration and is detailed in the actual circuit diagram.

D) <u>Multiplier</u>: The process of multiplication can be done using either a four quadrant multiplier or a balanced modulator. However the disadvantage with the available balanced modulators is that output signal level is small and hence further amplification is needed. Hence a four-quadrant multiplier XR-2208 is used in its phase-sensitive detection mode as shown in Fig. 4.4.

$V_\emptyset$ in this case is given by:

$$V_\emptyset = K_d \cos \emptyset$$

where $K_d$ is the phase detector conversion gain. If $K_d \geq 50$ mV r.m.s., $K_d = 2V/radian$. However, if input signals are <50 mV rms, then $K_d$ changes as the input changes. However, the output from Fig. 4.4 is differential in nature and hence a difference amplifier must follow. Again LM318 was found quite satisfactory for this purpose.
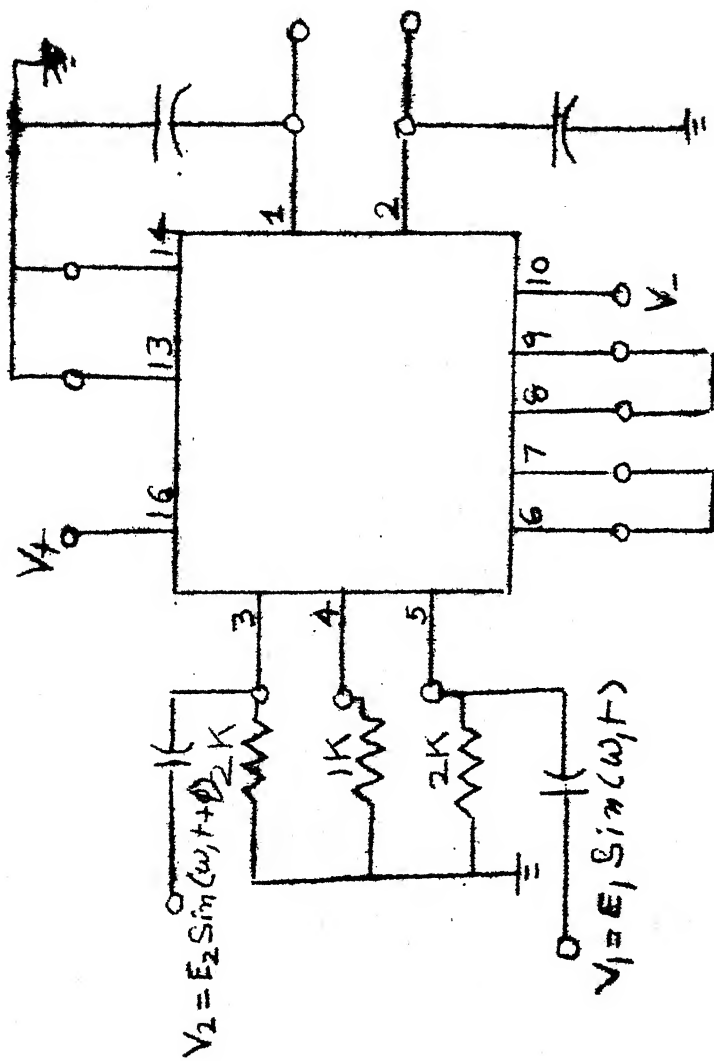
Fig. 4.4: XR-2208 as phase sensitive detector.

$V_2 = E_2 \sin(\omega_1 t + \phi)$

$V_1 = E_1 \sin(\omega_1 t)$

Since $K_d$ is small, its amplitude is increased by amplifying the reference signal in reference channel since any way on that channel, signal has to be larger than 50 mV r.m.s. The signal circuit then looks like as in Fig. 4.5.

## 4.4 DESIGN OF CURRENT TRANSIENT MEASUREMENT MODULE:

Current transient measurement module has two features different from that of capacitance measurement module in previous section. One is that one need not work at high frequencies in this case and second that level of signals is smaller in this case than of capacitance transients. The latter is particularly true since now it is the reverse bias current, which has to be monitored. In silicon diodes, this current is of the order of a few nanoamperes. Again due to requirements of Fritz's law, the first current to voltage converter should be as noise free as possible. The block diagram of such a setup is in Fig. 4.6. A brief description of each block is provided.

a) <u>I/V Converter</u>: This stage should be as noise free as possible. Hence a FET input low noise OPAMP is used. CA3140 is characterized by low offset voltage, low offset current high CMRR and high input impedance. Several stages of transimpedance are provided.
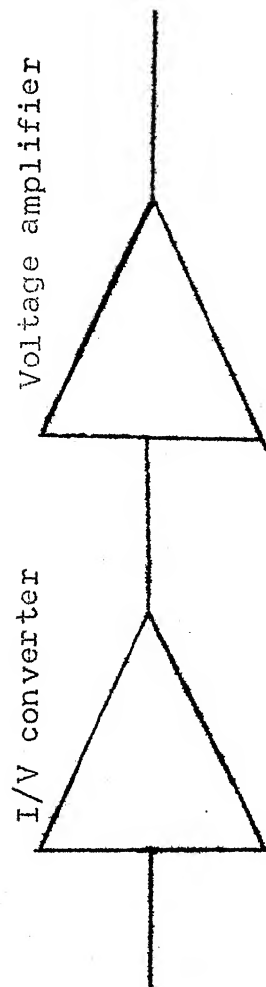
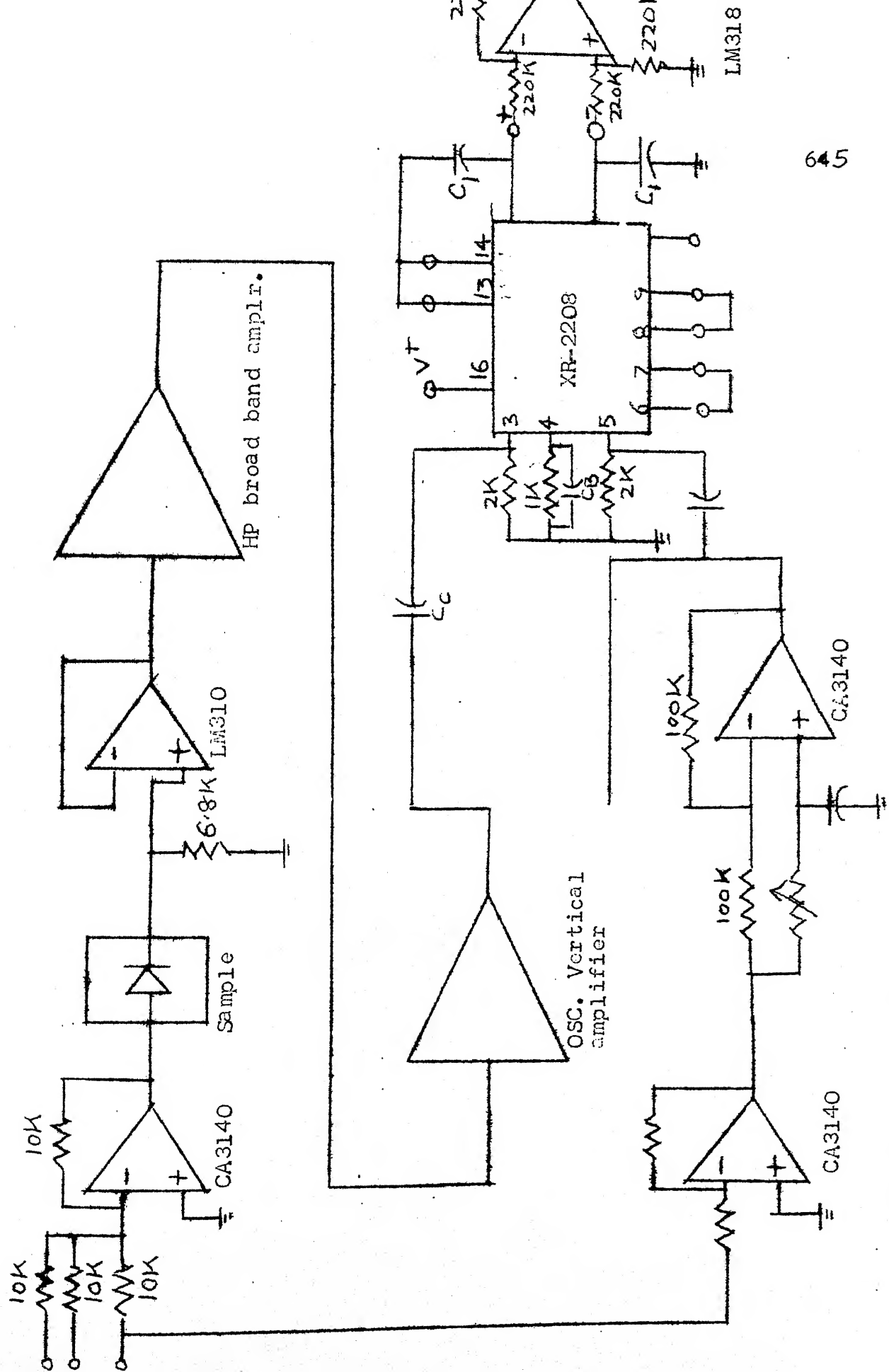Fig. 4.6: Block diagram of current measurement set up.

Fig. 4.5: Final circuit diagram for capacitance transient measurement
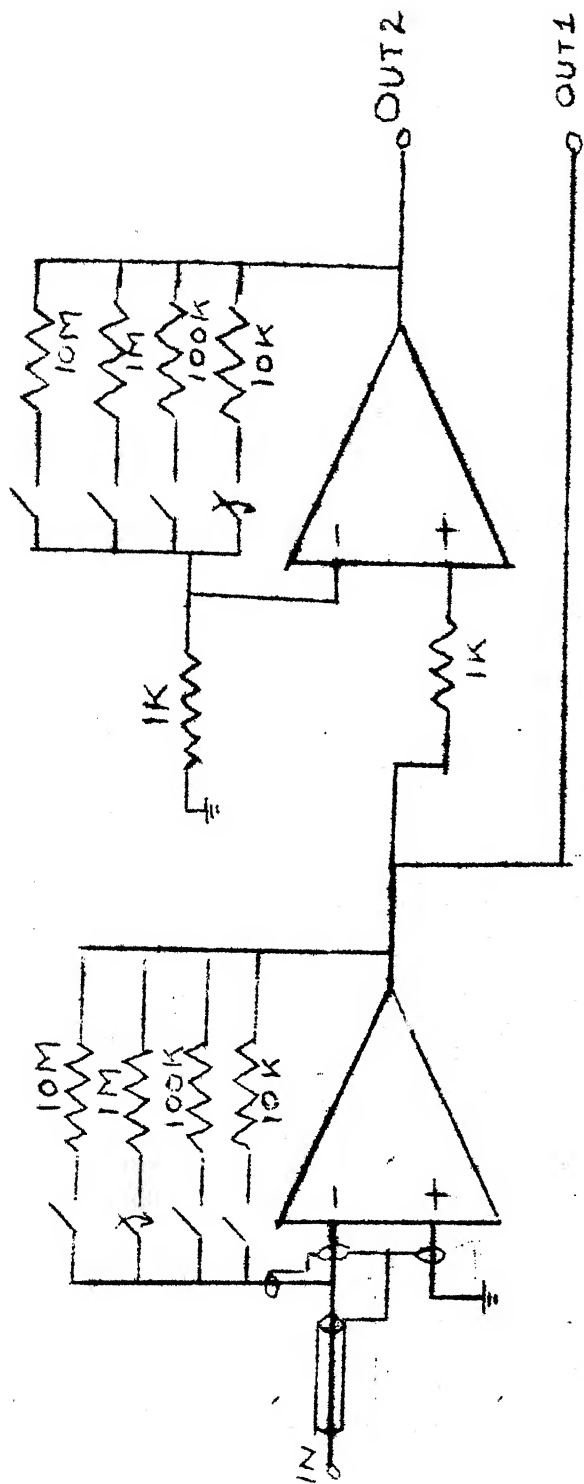
645

Fig. 4.7: Final current transient measurement circuit

b) <u>Voltage amplifier</u>: Again an amplifier with low noise, low offset current and voltages should be used. Multiple gains are provided in this case, too.

The final current transient circuit is as shown in Fig. 4.7. Some very important precautions need to be taken regarding:

    a) layout and connections

    b) selection of passive components

For layout, the above low noise, low level current transient set-up or electrometer should have proper shielding and guardrings must be provided to avoid loss of signal [13,14]. Both capacitance and current transient signal measurement setups have been developed and used to acquire these transients from a $P^+N$ junction diode. The details of this are in Chapter 5.

# CHAPTER 5

## EXPERIMENTAL RESULTS AND DISCUSSION

### 5.1 INTRODUCTION:

In this chapter the details of current and capacitance transients from commercially available Gold doped $P^+N$ junction diode have been given. These transients have been analysed to obtain the values of activation energy and capture cross-section related to Gold acceptor in silicon. The details are described below:

### 5.2 CURRENT TRANSIENTS:

The experimental system used to measure current transients has already been described in Fig. 4.1. A total of eighteen such transients spanning a temperature range of $110^0$K from $236^0$K to $274^0$K are taken and those at two temperat are shown in Fig. 5.1 and

/waveshapes are similar to the theoretically predicted one in Fig. 2.4. Before analysing these for determination of activation energy and capture cross-section, following considerations, over and above those already described for the measurement system of Fig. 4.1 are taken.

1. Each of the transients is measured using a majority carrier pulse wherein the voltage switches from 0 V to a reverse voltage $-V_R$. To illustrate the shape of pulse bias, the

majority carrier pulses in case of transients at $T = 251^{\circ}K$ and $T = 274^{\circ}K$ are shown in Fig. 5.1.

2. It has been found that pulse bias at a single frequency cannot be used for the complete temperature range used. This is because at lower temperatures, the time of decay of current transients are so large that it does not totally become zero, leading thus to conditions for DDLTS (Double DLTS). In such a case the analysis needs to be changed accordingly. On the other hand at high temperatures, the decay is so fast that a set of indistinguishable transients are obtained close to the negative going transition of bias pulse. Therefore for higher temperatures, high repetitive rate pulses are used and for lower temperatures, the repetitive rate is made so large that the decay is complete. This particular point is illustrated in Fig. 5.1 where the transient at $T=274^{\circ}K$ is measured using a pulse of about 2.40 ms period and one at $T=251^{\circ}K$ obtained with about 85 ms pulse period.

The transients obtained are submerged in noise. Hence the signal averaging capability of the signal analyser is used to increase SNR for these transients and it has been found that at least five hundred such averagings are necessary.
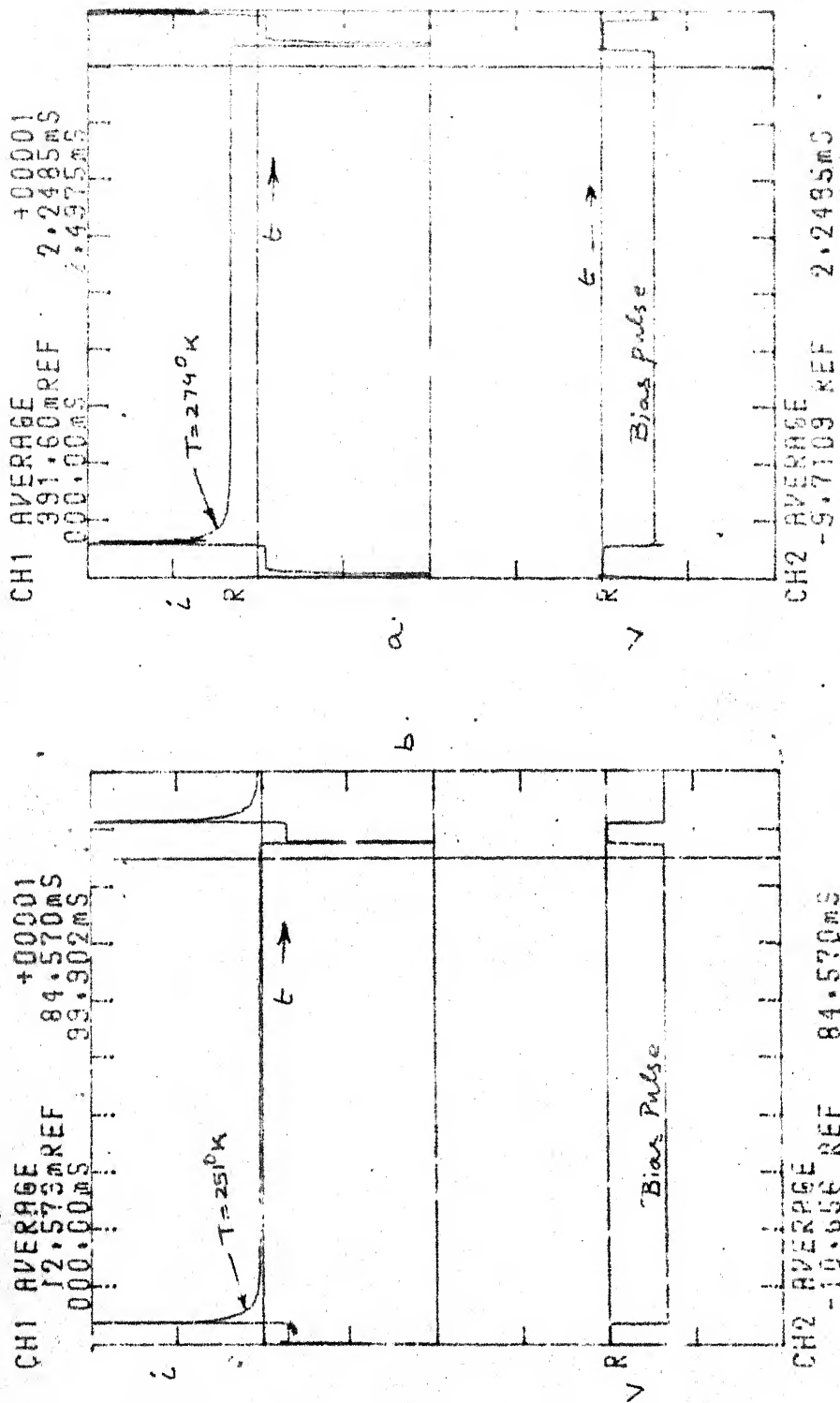
Fig. 5.1: Current transients at two different temperatures on a given majority carrier pulse sequence.

Before analysing the data, it is necessary to check out some features of current transients which are predicted by the eqn. (2.26). These are:

a) that the decay constants of the current transients decrease with decreasing temperature and

b) that the initial amplitude becomes smaller as the temperature is lowered.

Property (a) above is verified in Fig. 5.2 where the current transient signals at three different temperatures ($T=346^{\circ}K$, $325^{\circ}K$ and $T=306^{\circ}K$) have been plotted. In Fig. 5.2(a), $T=325^{\circ}K$ and $T=346^{\circ}K$ transients are compared and values are read by cursor at t = 261.23 μs to show a higher value of 826.43 mV for $T=346^{\circ}K$ transient meaning thereby that lower amplitude for latter transient is due to its faster decay. Similarly Figs. 5.2(b), 5.3(a) and (b) illustrate this property.

Theproperty (b) above can be observed by comparing the order of magnitudes of transients in Fig. 5.2 with those in Fig. 5.3. For instance at the cursor setting of t=261.23 μs in Fig. 5.2, the magnitudes are in hundreds of millivolts while in case of Fig. 5.3 at t=8.0078 ms setting of cursor, the magnitudes are in terms of millivolts. The temperatures in Fig. 5.3 are lower than temperatures in

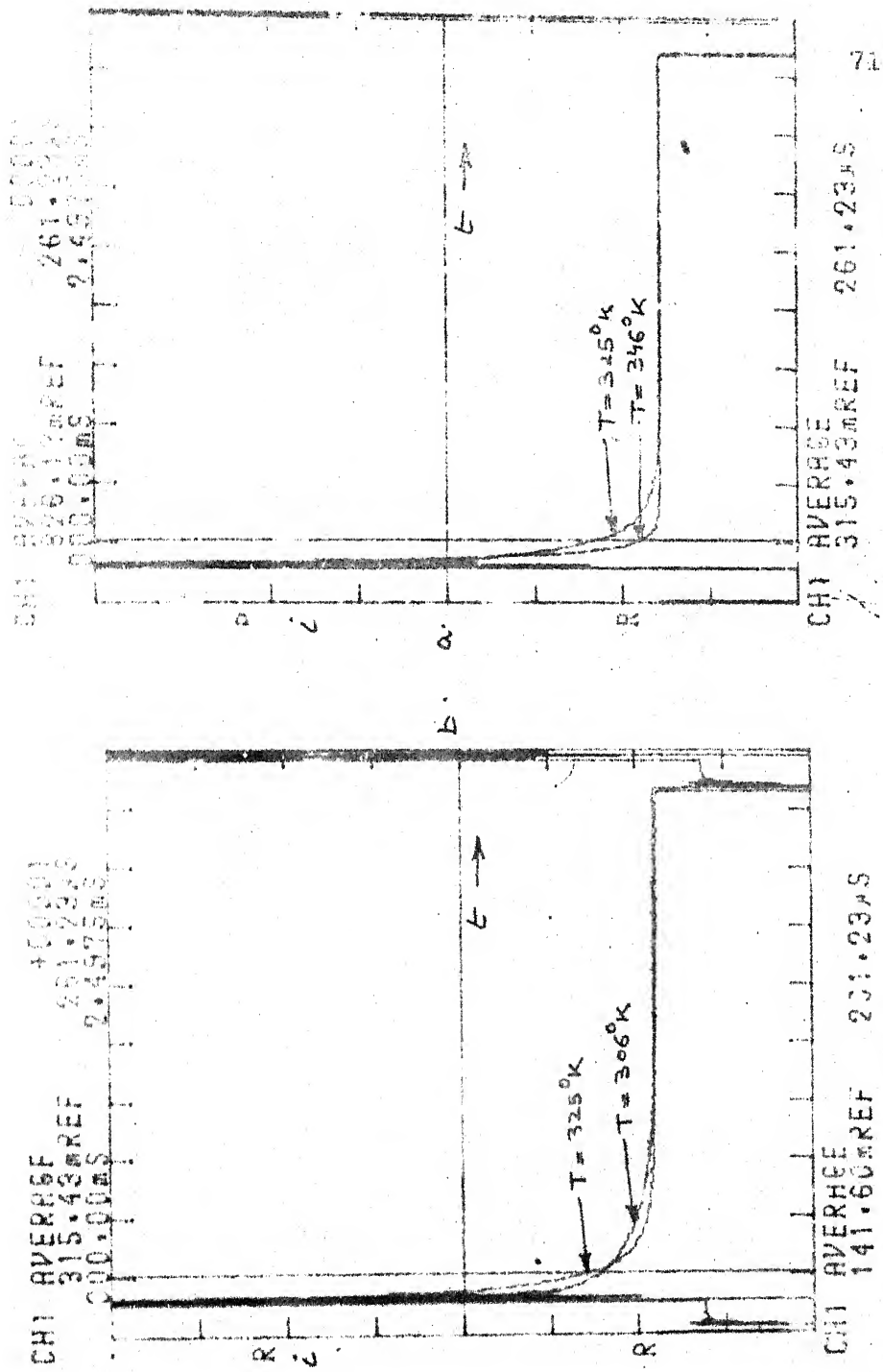Fig. 5.2: Comparison of current transients at different temperatures on a given majority carrier pulse sequence.

CH1 AVERAGE    +00000!
14.770mREF    8.0078mS
000.00mS      99.902mS

$T = 283°K$
$T = 269°K$

CH1 AVERAGE   6.0078mS
9.7656mREF

CH1 AVERAGE   +00000!
9.7656mREF    8.0078mS
000.00mS      99.902mS

$T = 266.4°K$
$T = 283.0°K$

CH1 AVERAGE   8.0078mS
6.8003mREF

Fig. 5.3: Comparison of current transients at two different temperatures on a given majority carrier pulse sequence.

72

Fig. 5.2, meaning hence that amplitudes decrease with temperature.

## 5.2 ANALYSIS FOR CURRENT TRANSIENTS:

The eighteen transient signals experimentally obtained have been analysed for determination of activation energy and capture cross-section. Many of the methods [4], [5], [8], [10] including the DLTS assume that the transients are single exponential. In practice it has been found that sometimes multiexponentials occur. Hence efforts should be made to find whether the transients are single exponential or not. The method described in Chapter 3 for multiexponential analysis is used for the first time to get this preliminary information. In case the signal shows single exponential behaviour, then either DLTS or any of the other single exponential analyses can be used. If it is multiexponential, then this algorithm itself can be used to get Arrhenius plot.
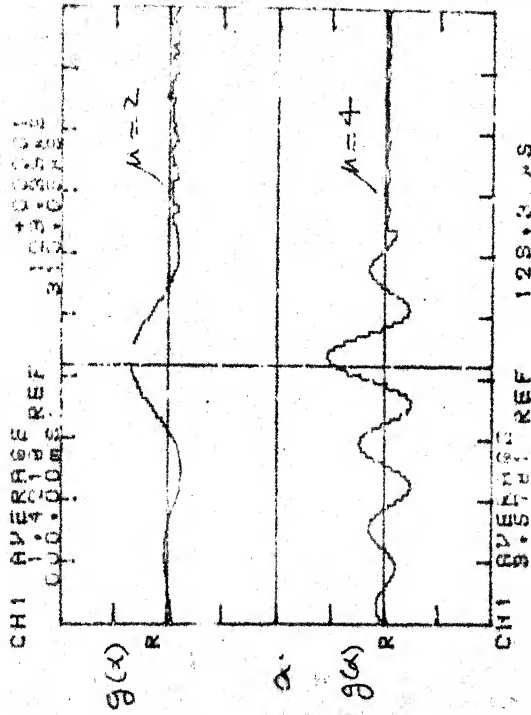
Therefore our analysis of current transients starts with multiexponential analysis of these transients. The details of this are given below:

a. Multiexponential analysis:

Herein the analysis is done at two temperatures. The current transients at 321.63°K and 258.5°K are chosen for
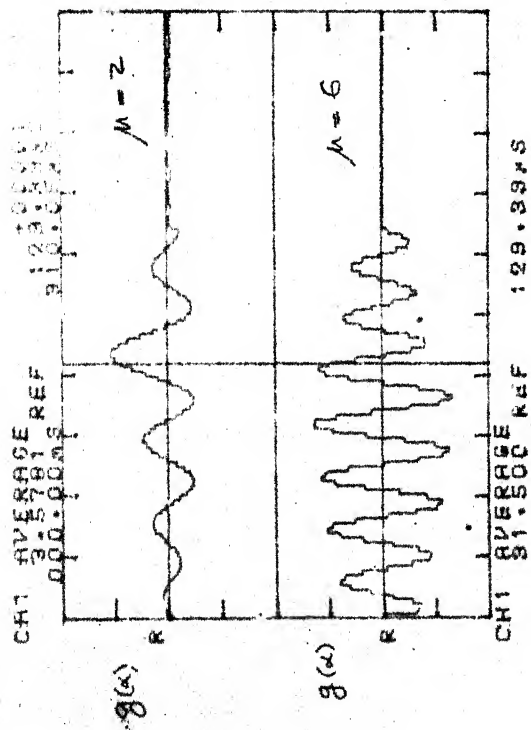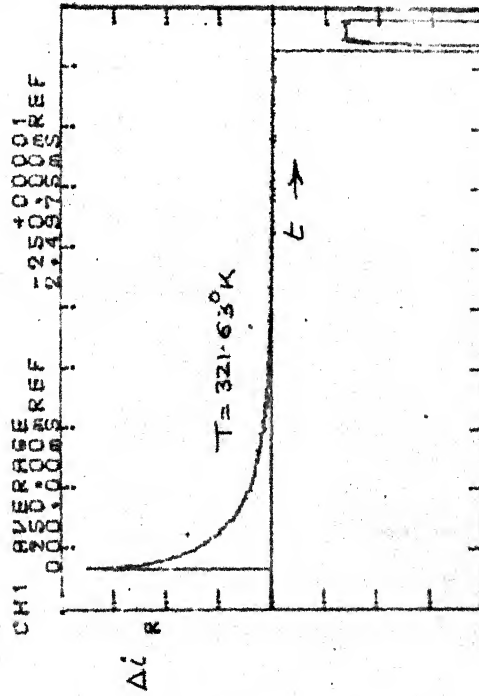
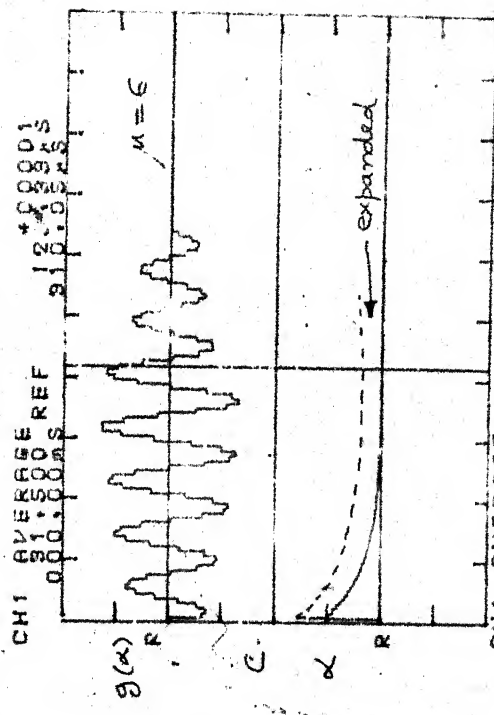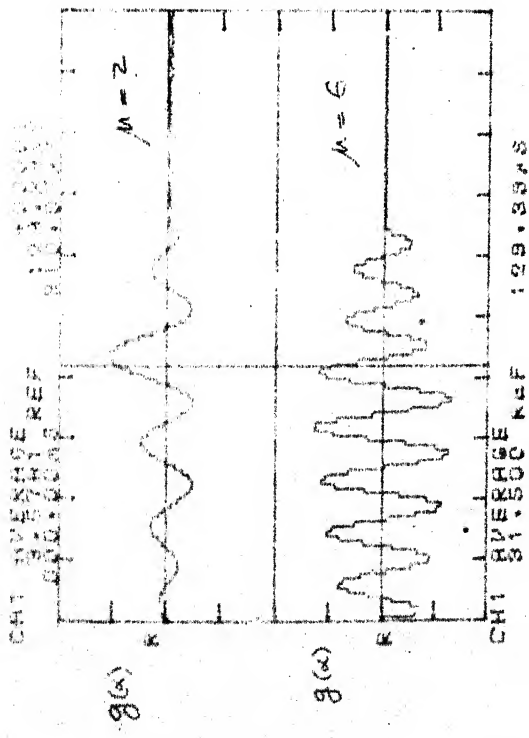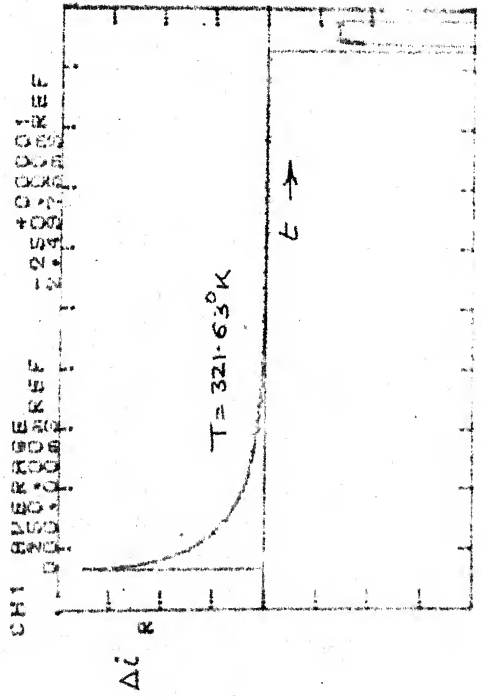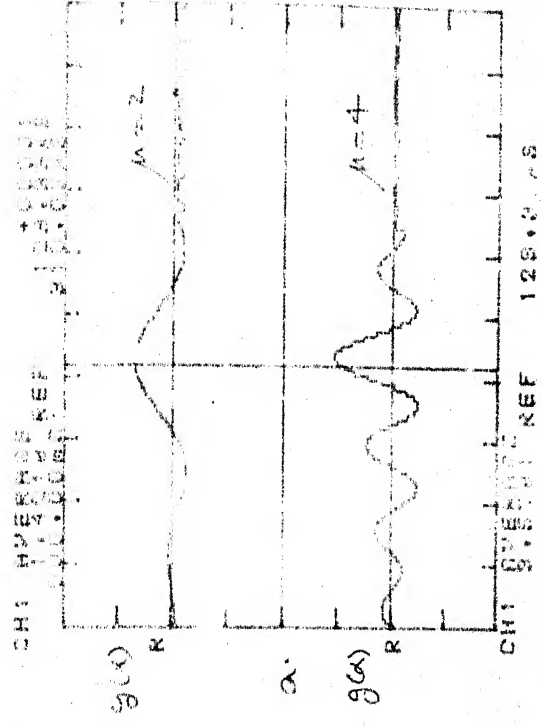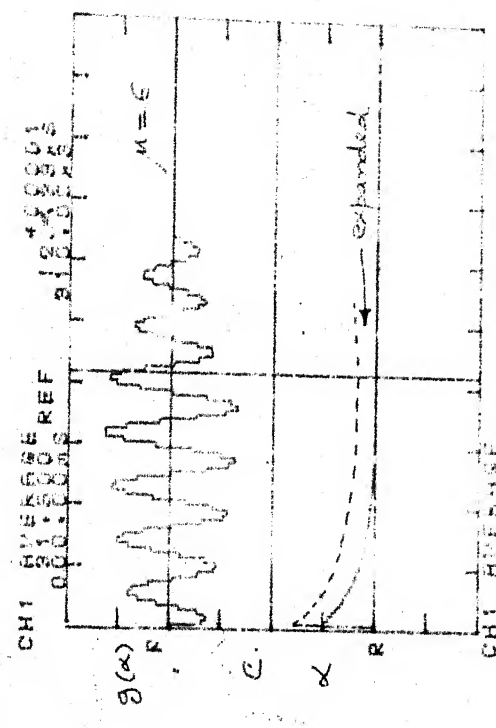Fig. 5.4: Multiexponential analysis of current transient at T=321.63°K.

75

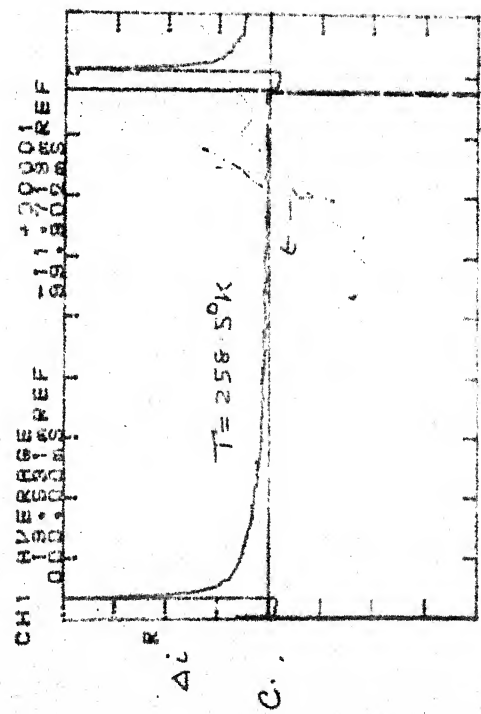Fig. 5.4: Multiexponential analysis of current transient at T = 321.63°K.

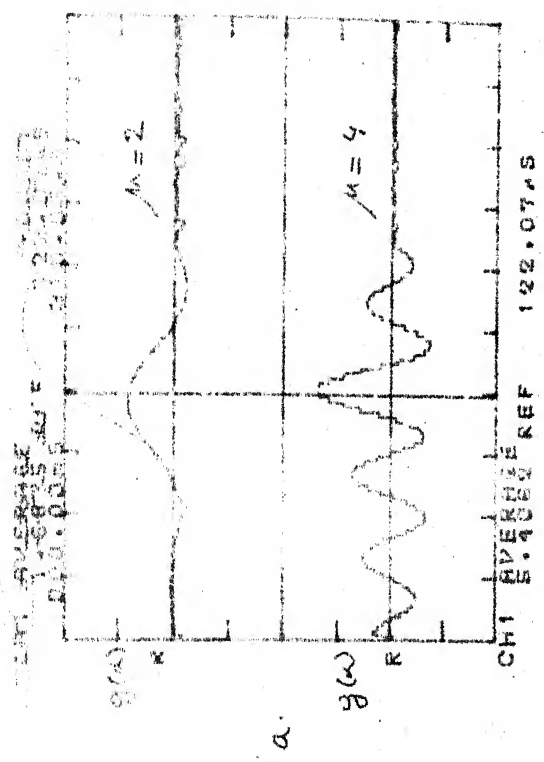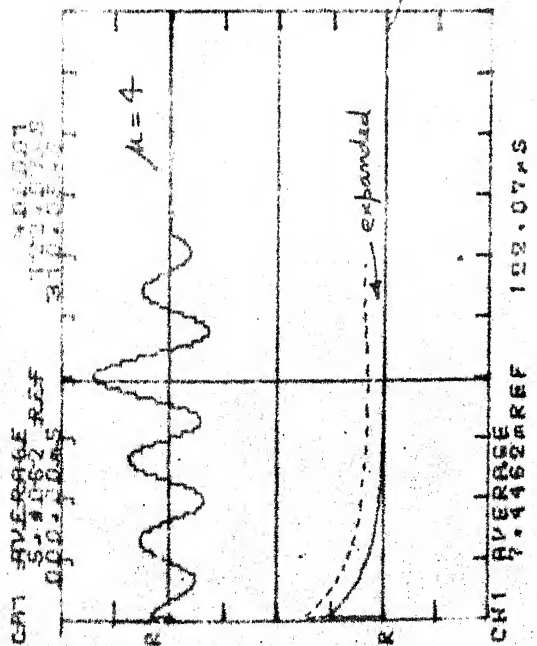Fig. 5.5: Multiexponential analysis of current transient at T=258.5°

specifically this effect is illustrated in Fig. 5.6(a) and (b) at two different temperatures.

2. Because of the above mentioned problem, using arguments of chapter three, area method is used to find values of B. These values for each temperature are given in Table 5.1. As can be seen, the values of B decrease with lowering of temperature, because it is due to leakage current which is temperature dependent.

3. The values of $\alpha$ and A are obtained from the original curve minus the value of B (i.e. $Ae^{-\alpha T}$). The program for this is provided in Appendix I. The values of A and $\alpha$ are also tabulated in Table 5.1. The values of both decrease with decreasing temperature according to eqn. (2.26).

4. These values of $\alpha$ with corresponding temperatures T are used to obtain the Arrhenius plot. As mentioned in Chapter 2, the slope of this plot gives the activation energy and intercept the capture cross-section. The values as obtained from the graph are shown therein.

5. The above values of $\alpha$ and $1/T$ are also fitted by a linear regression algorithm provided in Appendix I. The values of E, the activation energy and $g\,\sigma_n$, the capture cross-section are shown in Table 5.2.
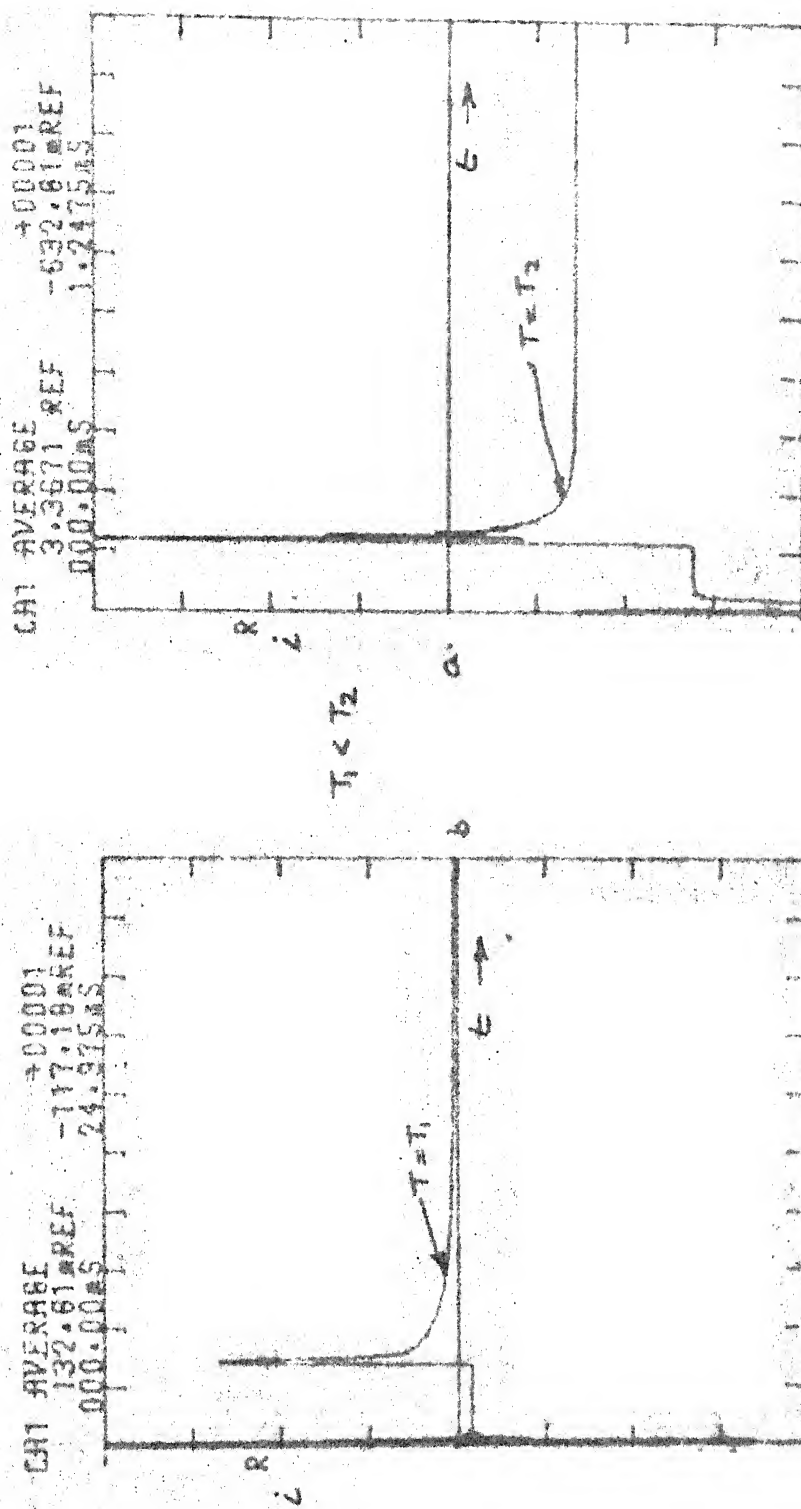
Next we discuss the capacitance data:

Fig. 5.6: Initial jitter in current transients.

Table 5.1: Current Transient Data

| DVM reading in mV | $t$ ° | $t+t_{amb}$ °C ($t_{amb}=26.5$°C) | $T$ °K | $\alpha$ | B | A |
|---|---|---|---|---|---|---|
| +1.903 | 46.90 | 73.40 | 346.4 | 29929.6 | +.793945 | .59091 |
| +1.750 | 43.41 | 69.80 | 342.8 | 26157.8 | +.647461 | .426551 |
| +1.408 | 35.17 | 61.67 | 334.67 | 20932.8 | +.395507 | .416720 |
| +1.033 | 26.09 | 52.59 | 325.59 | 13321.6 | +.217285 | .319616 |
| +C.875 | 22.175 | 48.675 | 321.675 | 11984.7 | +.167968 | .292027 |
| +C.747 | 19.0 | 45.5 | 318.5 | 9720.55 | +.134277 | .209612 |
| +0.565 | 14.45 | 40.95 | 313.95 | 7580.39 | +.93261x10$^{-1}$ | .181212 |
| +0.437 | 11.20 | 37.70 | 310.7 | 6805.17 | +.74707E-1 | .159619 |
| +0.283 | 7.30 | 33.8 | 306.8 | 5886.58 | +.571289E-1 | .146478 |
| -0.087 | -2.26 | 24.24 | 297.24 | 5130.87 | +.35644E-1 | .081954 |
| -0.229 | -6.00 | 20.50 | 293.50 | 3054.75 | +.217285E-1 | .074630 |
| -0.433 | -11.42 | 15.08 | 288.08 | 1888.84 | +.129394E-1 | .050473 |
| -0.604 | -16.00 | 10.00 | 283.00 | 699.077 | +.125732E-1 | .62037E-1 |
| -0.805 | -21.47 | 5.03 | 278.03 | 497.057 | +.94909E-2 | .148043E-1 |
| -1.133 | -30.58 | -4.08 | 268.92 | 244.117 | +.65307E-2 | .747719E-2 |
| -1.254 | -34.00 | -7.5 | 261.50 | 155.657 | +.56152E-2 | .540611E-2 |
| -1.490 | -41.00 | -14.5 | 258.5 | 69.0142 | +.42724E-2 | .264043E-2 |

Table 5.2: Experimental results

|  | Current transients | Capacitance transients |
|---|---|---|
| $\Delta E_{ev}$ | 0.529232 | 0.581456 |
| $g\sigma_{n}\ cm^{2}$ | $8.84469 \times 10^{-15}$ | $6.64321 \times 10^{-15}$ |

Arrhenius plot (current transients)



$\ln(e_1) \longrightarrow$

$\frac{1000}{30T}$

$\triangle E = 0.579 \, eV$
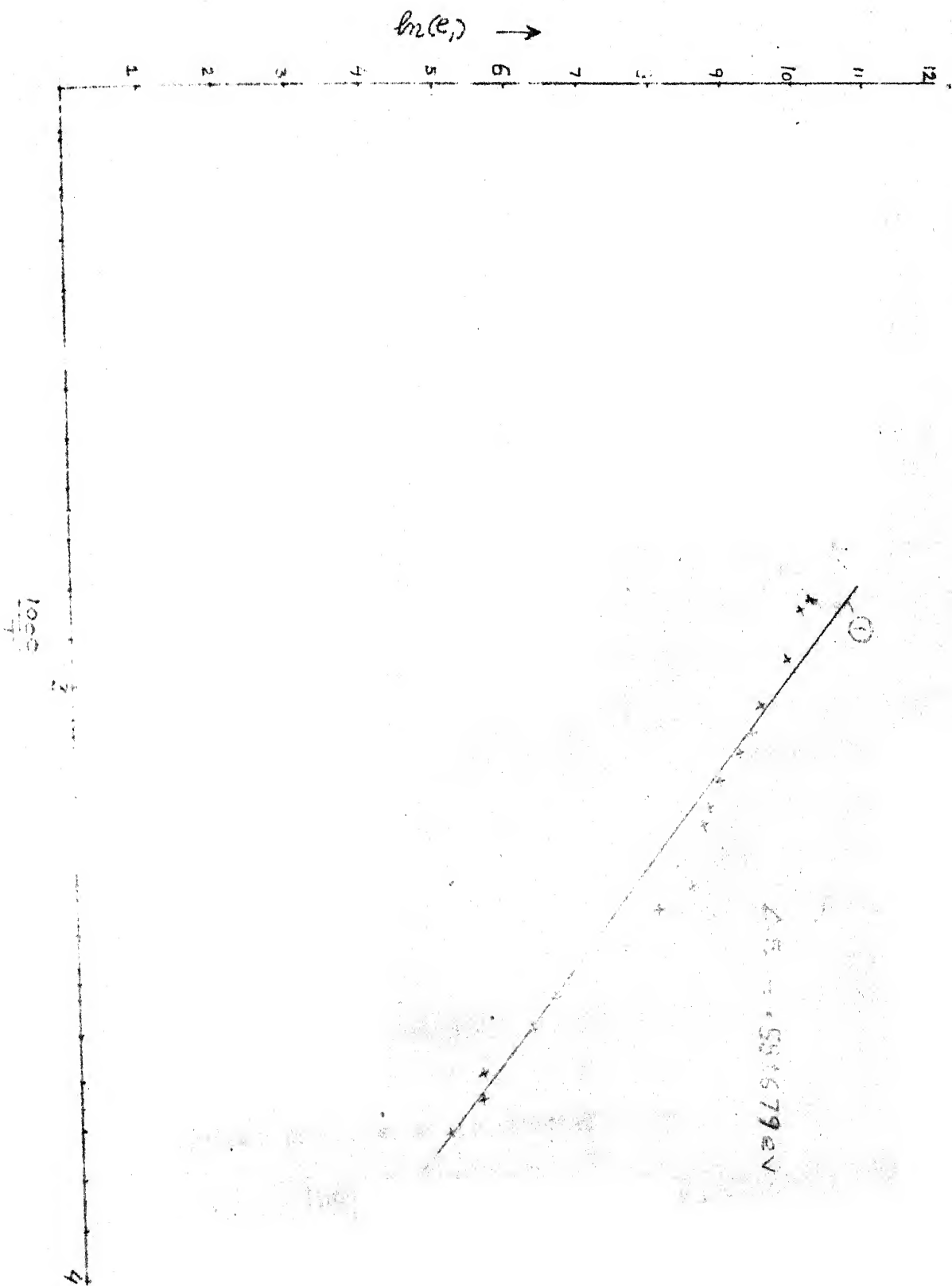
## 5.3 CAPACITANCE TRANSIENTS:

There is only one change while measuring the capacitance transients as compared to that of current transients. In the measurement system of Fig. 4.1, the current measurement set up is replaced by capacitance set up. A total of eleven measurements are made over a $50^{\circ}$K range from 298.9$^{\circ}$K to, 250$^{\circ}$K. The waveshape of typical capacitance transients is illustrated in Figs. 5.7 and 5.8. These waveshapes are found to be same as theoretically expected in Fig. 2.4. Both the considerations mentioned for current transients hold in this case too. This means that we have again majority carrier pulses, switching from 0 V to a reverse voltage $- V_R$. This is illustrated in Figs. 5.7 and 5.8, where the pulse bias is shown below the capacitive transients at four different temperatures. Due to the same difficulties as faced in current transients,a set of different repetition rates are use For the highest temperature of these at T=292.71$^{\circ}$K the pulse period is about 9.0 ms and for the lowest temperature T = 246$^{\circ}$K illustrated in Fig. 5.8(b), the pulse period is 90 ms. The intermediate two temperatures similarly have pulse periods of 16 ms and 45 ms.

The capacitance transients are again very noisy and at each of the temperatures multipoint averaging is done to get cleaner signal. The effect of noise is more at lower
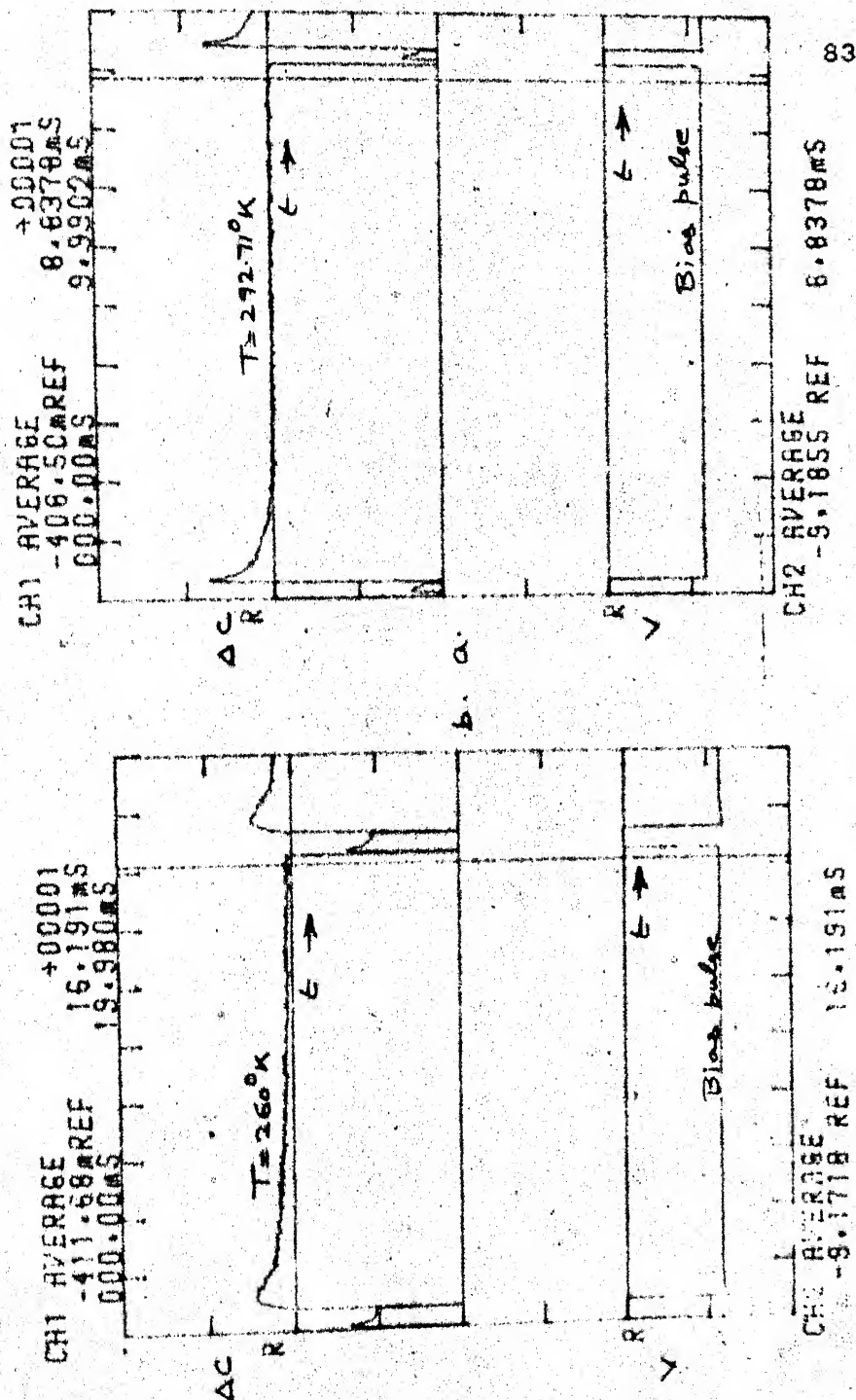
Fig. 5.7: Isothermal capacitance transients at two different temperatures on a given majority carrier pulse sequence.
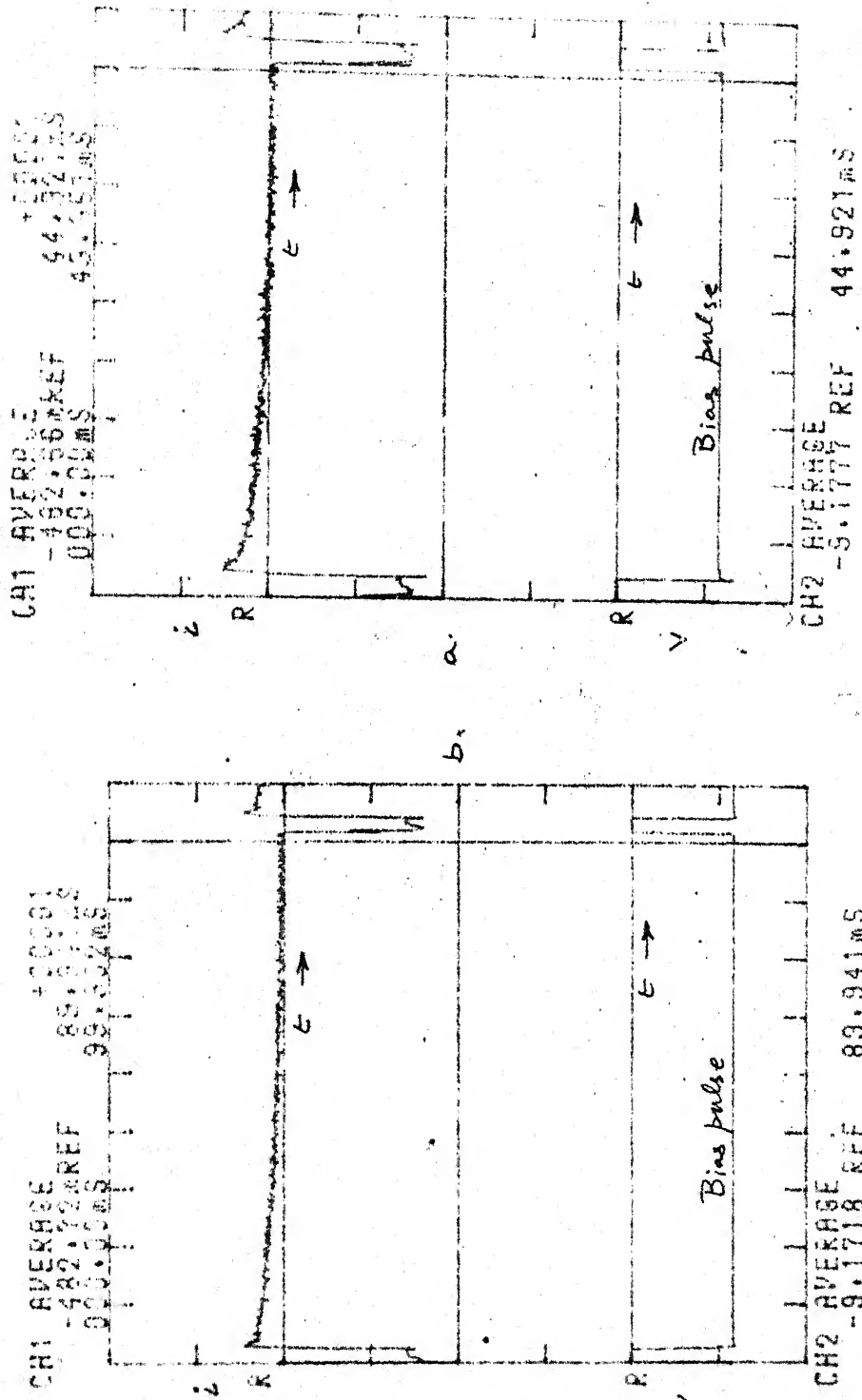
Fig. 5.8: Isothermal capacitance transients at two different temperatures on a given N majority carrier pulse.

84

temperatures when signal strength becomes small. This effect can be observed in Figs. 5.7(b), 5.8(a) and (b) and Fig. 5.9(b).

In this case too, we check the capacitance transients for some features predicted by eqn. (2.19). These are:

    a. that the decay time increases as the temperature is decreased

and  b. that the initial amplitude remains constant.

Property (a) is verified in Fig. 5.8(a) and (b) and Fig. 5.9(a). In Fig. 5.8(a), the capacitive transients at $T = 298.8^{O}K$ and $T = 288.43^{O}K$ are compared with each other. At the setting of the cursor at $t = 830.07$ $\mu s$, the values read are 88.195 mV and 91.735 mV respectively, meaning thereby that the transient at $T=298.87^{O}K$ decays faster than at $T=288.43^{O}K$. The same effect can be seen at other comparisons shown in Figs. 5.8(b) and 5.9(a).

Property (b) can again be verified in Fig. 5.8(a) and (b), where initial amplitudes are found equal.

We proceed next with the analysis for determination of activation energy and capture cross-sections.

5.3.2 Analysis for Capacitive Transients:

Here again as in current transients, a serious need is felt to verify if the capacitive transients are single
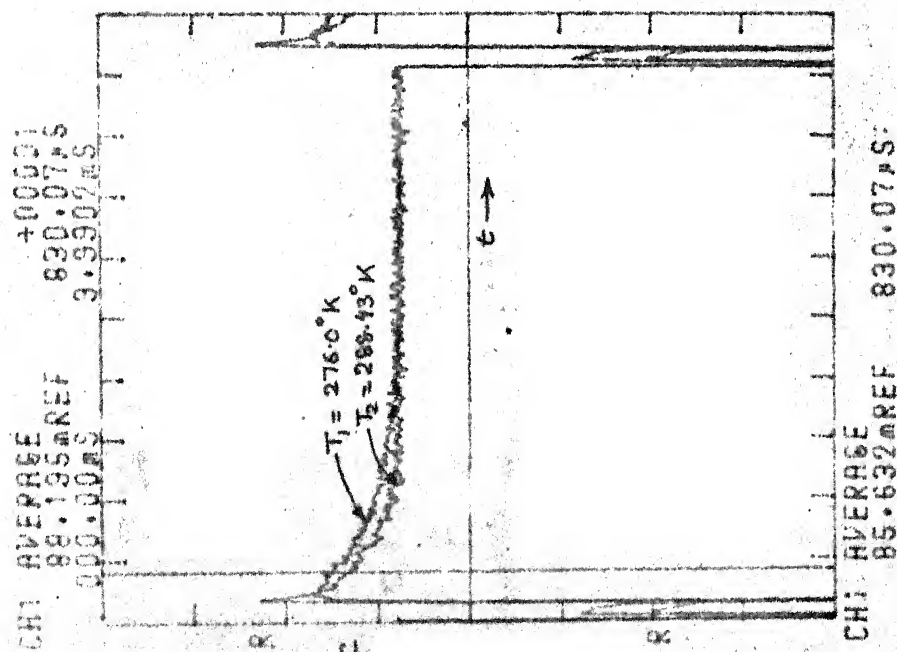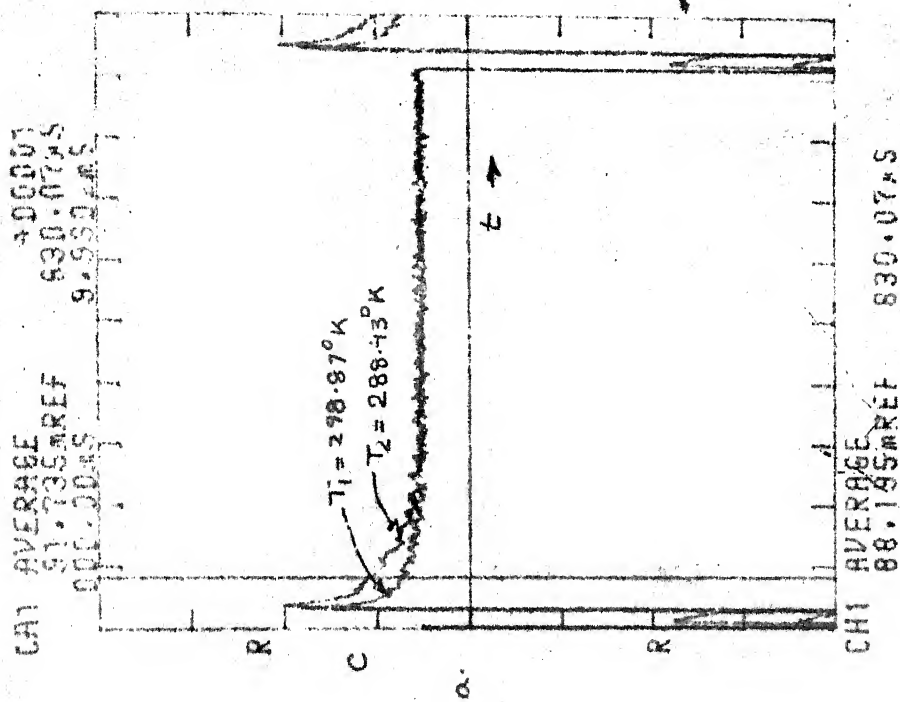
Fig. 5.8(2): Comparison of capacitance transients at two different
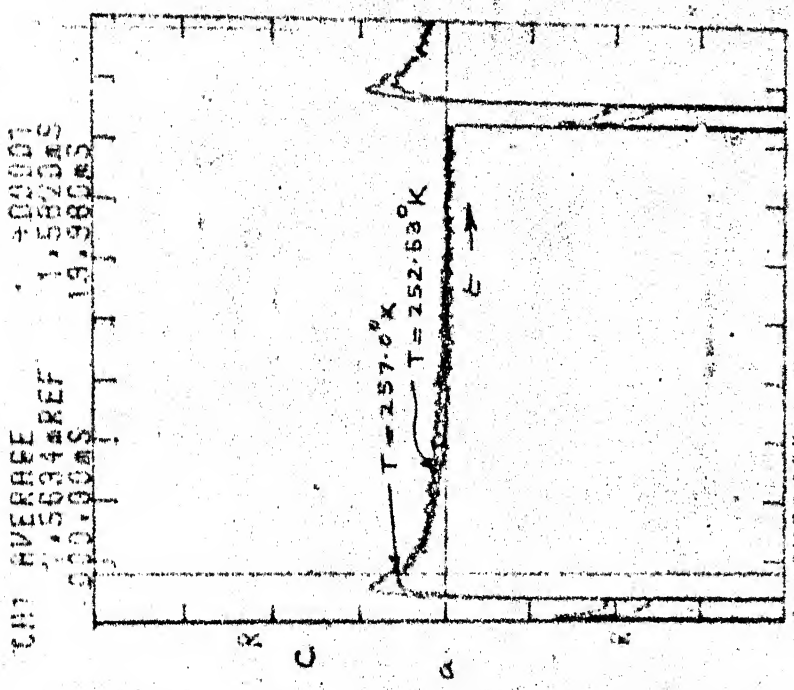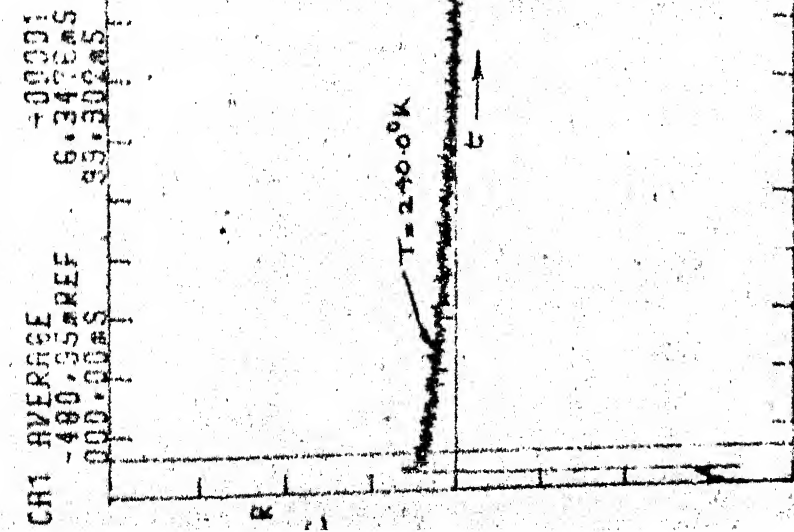temperatures on a given majority carrier pulse sequence.

Fig. 5.9 a: Isothermal capacitance transient at T=240.0°K.
b: Comparison of two capacitance transients at two different temp.
on a given majority carrier pulse sequence.

exponential or not so that either DLTS or any of the other single exponential analysis could be used or not. Therefore the multiexponential analysis is done to verify the existence of the single exponencity. In case the transients are single exponential, then either DLTS or any of the other single exponential analyses can be used. If, however, these are multiexponential, then this algorithm can be itself used to get Arrhenius plot.

Therefore our analysis of capacitance transients starts with multiexponential analysis. The details of this are given below:

a. Multiexponential analysis:

The capacitance transients at two temperatures are analysed for multiexponencity. These transient are at $T=252.53^{\circ}K$ and $T=279.61^{\circ}K$ and are shown in Figs. 5.10(d) and 5.11(c) respectively. The multiexponential algorithm when applied to transient at $T = 279.61^{\circ}K$ gives for $\mu=2$, $\mu=4$ and $\mu=6$ in (a) and (b) and its value can be read in Fig. 5.10(c) as 1489. This the transient at $T=279.61^{\circ}K$ has single exponential.

Similarly the capacitance transient at $T=252.53^{\circ}K$ is analysed for multiexponents. The results of this are shown in Fig. 5.11 where (a) and (b) give the $g(\alpha)$ values for

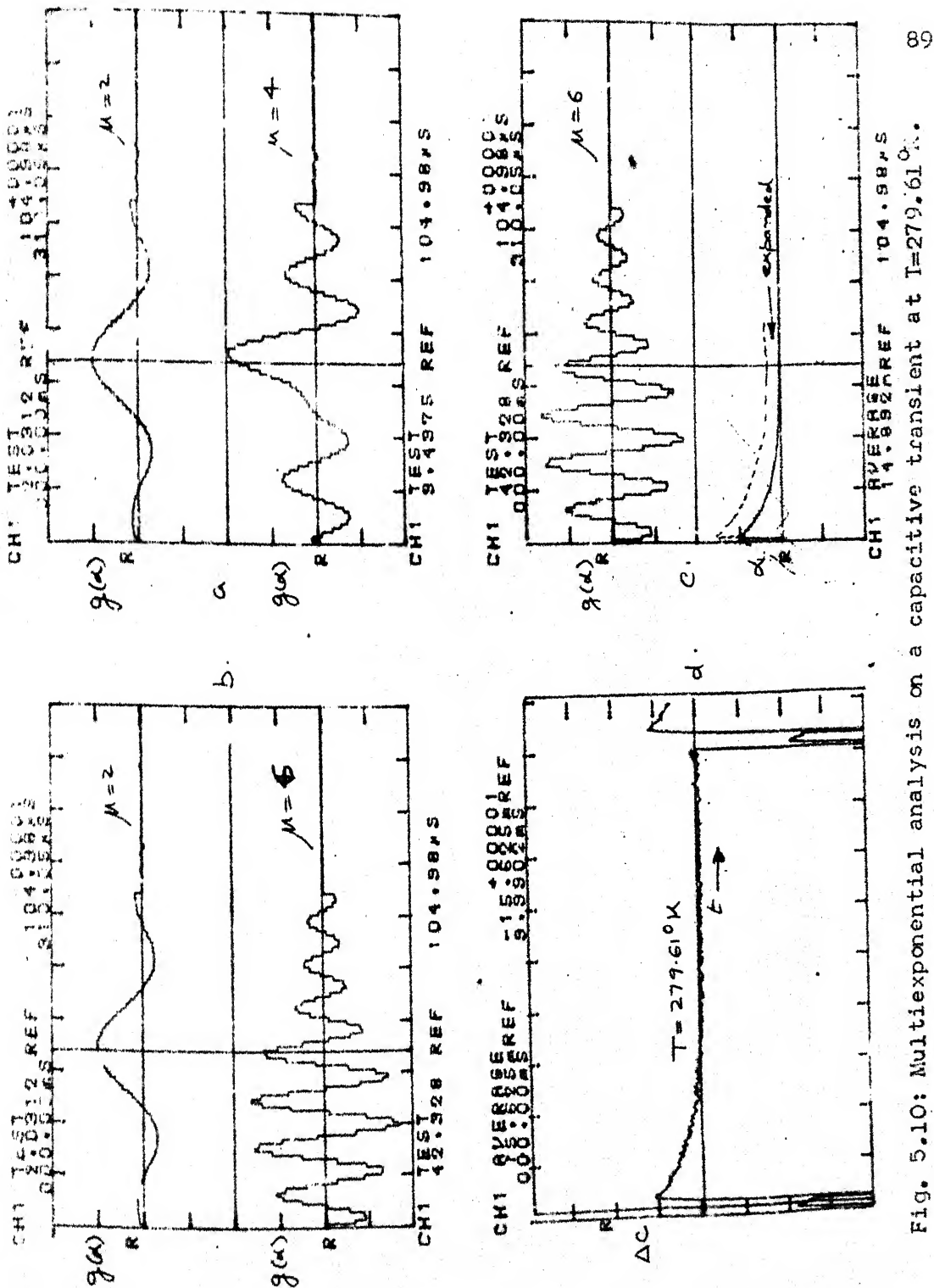Fig. 5.10: Multiexponential analysis on a capacitive transient at T=279.61°K.

$\mu=2$, $\mu=4$ and $\mu=6$. One particular peak is seen to remain constant and the $\alpha$ value at this is read at the cursor point in Fig. 5.11(c). The value found for $\alpha$ is 135.49. Hence the capacitive transient at T=252.53$^{\circ}$K is also single exponential.

The reason why only two temperatures are analysed for multicomponents is that the multiexponential analysis in its present implementation takes long time. Having verified that the transients are single exponential, any of the simpler and faster single exponential analyses can be used to find the values of decay constants. It is described below.

b. Single Exponential analysis:

Here the capacitive transients are assumed to have the form $Ae^{-\alpha t} + B$. The following steps are taken to get values of A, $\alpha$ and B.

1. The Area method is again used to find values of B. These values of B are tabulated for a few temperatures in Table 5.3. As can be seen that this value is essentially constant because the capacitance at steady state reverse bias is same at all temperatures. These values of B are removed from the whole waveforms at each of the eleven temperatures.

2. The modified waveforms now obtained are of the form $Ae^{-\alpha t}$ and values of $\alpha$ and A are determined using ratio of the

Table 5.3: Capacitance Transient Data

| DVM reading in mV | $t_o$ | $t+t_{amb}$ $t_{amb}=25°C$ °C | T °K | $\alpha$ | B | A |
|---|---|---|---|---|---|---|
| +0.033 | 0.87 | 25.87 | 298.87 | 9000 | .91475E-1 | .51395E-2 |
| -0.202 | -5.29 | 19.71 | 292.71 | 5151 | .904306E-1 | .625014E-2 |
| -0.364 | -9.57 | 15.43 | 288.43 | 3998 | .861206E-1 | .60253E-2 |
| -0.521 | -13.76 | 11.24 | 284.24 | 2601 | .86029E-1 | .55721E-2 |
| -0.692 | -18.39 | 6.61 | 279.61 | 1640 | .851276E-1 | .445931E-2 |
| -.978 | -26.25 | -1.25 | 271.75 | 428 | - | - |
| -1.495 | -40.94 | -15.94 | 257.00 | 220 | - | - |
| -1.651 | -45.47 | -20.47 | 252.53 | 138 | - | - |
| -1.874 | -52.00 | -27.0 | 246.00 | 60 | - | - |
| -2.045 | -47.24 | -32.24 | 240.76 | 35 | - | - |

Arrhenius plot (Conductance transients.)
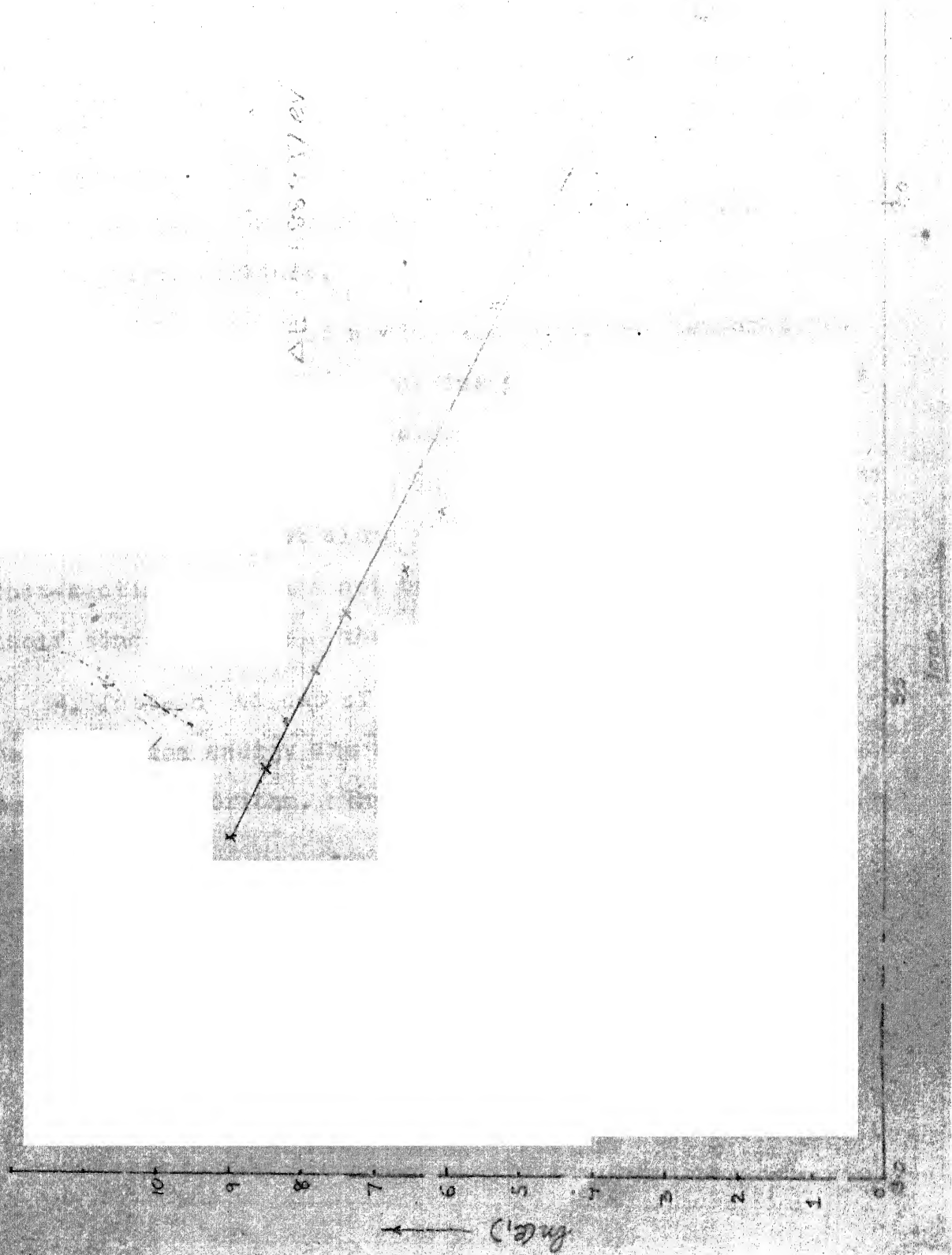
exponential function at two instants. These values of A and $\alpha$ are also given in Table 5.3. The value of A does show small change and it is both because of quantization error as well as the actual high frequency cut off in the signal analyser. The $\alpha$ values show a decrease, with decrease in temperature.

3. These values of $\alpha$ with corresponding temperatures T are used to obtain the Arrhenius plot. The slope of this plot gives the activation energy of the acceptor level of Gold in silicon and is given in the plot itself. Though the intercept of this plot along the ordinate gives capture cross-section, this has not been got on the Arrhenius plot itself since the plot, then extends outside the graph.

4. Instead values of the capture cross-section and the activation energy are accurately computed by linear regression algorithm. These results are tabulated in Table 5.2.

A comparison of these measured values with the ones published in literature is given in the next chapter.

# CHAPTER 6

## CONCLUSION

The values of the activation energy $\Delta E$ and capture cross-section $g\,\sigma_n$ of gold acceptor level in gold doped silicon $P^+N$ Junction diode 1N4148 have been measured using majority carrier pulses. The values of $\Delta E$ using isothermal current transient study (ITS) and using isothermal capacitance transient study (CTS) have been found to be $\approx 0.53$ eV and

0.58 eV respectively. These values are well within the published values which vary from 0.52 to 0.58 [10]. Similarly the values of $g\,\sigma_n$ found by ITS and CTS are $\approx 0.8845 \times 10^{-14}$ cm$^2$ and $0.664.321 \times 10^{-14}$ respectively . These $g\,\sigma_n$ values are found well within those published and which vary from $9.0 \times 10^{-17}$ cm$^2$ to $2.5 \times 10^{-15}$ cm$^2$ [16]

Current and capacitance transients were obtained using especially designed measurement set ups capable of acquiring low level current and capacitance signals.

A multiexponential analysis algorithm was used to help detect the multiexponents in relaxation data.

Some limitations of the above work and ways to improve these are as follows:

The multiexponential analysis, as implemented in our case, realizes Fourier transforms through numerical integrations. This means that an increase in execution time as well

as in numerical errors.  If the FFT routine of the signal analyser can be used, then both the above problems can be solved.

An error analysis is particularly desirable for the multiexponential analysis.  This is because the signal from the form $\sum_{i=1}^{n} A_i e^{-\alpha_i t} + B$ is reduced to $\sum_{i=1}^{n} A_i e^{-\alpha_i t}$ using Area method.  The effect of such a step needs to be determined.

The multiexponential analysis has the limitation that $A_i$ should decrease with a decrease in $\alpha_i$.  Due to long execution time of the program, the extent to which this condition is stringent could not be known.  With FFT implementation, it would be easier then to determine the extent of this limitation.

The current transient setup could be redesigned to remove the large current component.  The design is, however, slightly difficult since this fast transient decays is less than a few microseconds.

Finally the capacitance module has been found noisy. A better layout and better choice of less noisy components can help solve this problem.

# APPENDIX I

## I.A PROGRAM TO FIND EMISSION RATE CONSTANTS BY LINEAR REGRESSION ALGORITHM

```
  5    DIM X(500), Y(500)
  7    H = 2.4414E-06
  9    E3=50, E4=50
 10    J= = 55, J7 = 55
 12    T8 = 300
 15    T7 = 30
 17    FOR J = 1 TO T8
 20    X(J) = H*(J1-E3)
 30    T9 = B(2,0,J1)
 40    Y(J) = LN(T9)
 50    J1 = J1+1
 60    NEXT J
 65    S1 = 0, T1=0, S0=0, S2=0,T2=0
 70    FOR I=1 TO T7
 80    S1 = S1 + X(I)
 90    T1 = T1 + Y(I)
 95    S0 = S0 + X(I)* Y(I)
100    S2 = S2+X(I)*X(I)
110    T2 = T2+Y(I)*Y(I)
120    NEXT I
130    X1 = S1/T7, Y1=T1/T7, X2=S2/T7
135    Y2=T2/T7, P = S0/T7
140    P1=X2-(X1*X1), P2= Y2-(Y1*Y )
150    M = (P-X1*Y1)/P1
160    C=Y1-M*X1
165    PRINT 'E3', E3
170    PRINT 'M', M, 'C', EXP (C)
172    T4 = 0
175    FOR L=1 TO T4
```

```
180   Y(L) = M*X(L)+C
190   I1 = EXP(Y(L))
200   I2 = B(2,0,J7)
205   G = (I2-I1)
210   T4 + T4+G*G
215   J7 = J7+1
220   NEXT L
230   R4 = T4/T8
240   PRINT 'MSE', R4
250   E3 = E3+1
260   IF E3 < = E4 GO TO 10
270   STOP
```

I.B PROGRAM TO FIND EMISSION RATE CONSTANTS BY FINDING RATIO
     AT TWO TIME INSTANTS

```
  5   DIM D(20)
 10   E1 = ?
 20   TO = 2.4414E - 06
 30   K = 30
 40   X=E1
 42   I = 1
 45   Y = X+K
 60   TL = X* TO, T2, Y*TO
 70   Y1 = B(2,0,X), Y2=B(2,0,Y)
 80   XO = LN(Y1/Y2)/(T2-T1)
 82   D(I) = XO
 85   X = X+1
 90   PRINT I, XO
100   I = I+1
110   IF I < =4 GO TO 45
185   S = 0
190   FOR J=1 TO I
210   S = D(J) + S
215   P = S/6
```

```
220   PRINT P,S
230   STOP
```

I.C LEAST SQUARE FIT PROGRAM TO RELAXATION DATA FOR
   ARRHENIUS PLOT

```
 5    DIM X(20), Y(20)
10    T1 = 50.427, T2 = 44.95, T3 = 39.859, T4=33.6026,
      T5 = 27.8684
20    T6 = 20.3684, T7 = 14.04, T8=8.04, T9=4.06,
      Q1 = -2.16, Q2 = -6.90
30    Q3 = -12.186
35    E1 = 9881.65, E2=7125, E3=5378. 260, E4=3653.9,
      E5 = 2397.92
40    E6 = 1400.6834, E7=704.34, E8=384.03, E9=269.417,
      Z1 = 179.109
43    Z2 = 125.062, Z3=84.9573
45    K=1.0E-6
47    T = 273
50    X(1) = 1/(T1+T), X(2)= 1/(T2+T), X(3)=1/(T3+T)
      X(4) = 1/(T4+T)
55    X(5) = 1/(T5+T), X(6)=1/(T6+T)
57    X(7) = 1/(T7+T),X(8)=1/(T8+T)
59    X(9) = 1/(T9+T), X(10)=1/(Q1+T), X(11)= 1/(QZ+T),
      X(12)= 1/(Q3+T)
60    Y(9) = LN(E9), Y(10)=LN(Z1), Y(11)=LN(Z2),
      Y(12)= LN(Z3)
61    Y(1) = LN(E1), Y(2)=LN(E2)
62    Y(3) = LN(E3), Y(4)=LN(E4)
63    Y(5) = LN(E5), Y(6)=LN(E6)
64    Y(7) = LN(E7), Y(8)=LN(E8)
65    S1=0, T1=0,S0=0, S2=0,T2=0
67    S=12
70    FOR I=1 TO 12
```

```
80    S1=S1 + X(I)
90    T1=T1 + Y(I)
95    SO = SO+X(I)*Y(I)
100,  S2 = S2+X(I)*X(I)
110   T2 = T2+T2+Y(I)*Y(I)
120   NEXT I
130   X1 = S1/S, Y1 =T1/S, X2=S2/S
135   Y2 = T2/S, P= SO/S
140   P1 = X2-(X1*X1), P2=Y2-(Y1*Y1)
150   M = (P-X1*Y1)/P1
160   C = Y1-M*X1
170   PRINT 'M', M,'C',C
175   D=M*8.61E-5
177   V = (EXP(C))/(2.6E+26)
180   PRINT 'D', D, 'V', V
190   STOP
```

I.D PROGRAM TO FIND EMISSION RATE CONSTANTS USING RATIO
     METHOD

```
3     E1 = 56, E2=74, E3=98
5     TO = 2.4414E-6
7     T1=TO*E1, T2=TO*E2, T3=TO*E3
10    K=8
12    Y1=B(K,O,E1), Y2=B(K,O,E2), Y3=B(K,O,E3)
20    XO = 1000.0
30    P1 = (EXP(-XO*T1))
40    P2 = (EXP(-XO*T2))
50    P3 = (EXP(-XO*T2))
70    F1=T2*P2*(P1-P3)
80    F2 = T1*P1*(P3-P2)
90    F3 = T3*P3*(P2-P1)
100   D1 = (P3-P2)*(P3-P2)
110   D2 = (F1+F2+F3)/D1
```

```
120   E2 = ((P2-P1)/(P3-P2))
130   N1 = ((Y2-Y1)/(Y3-Y2)
140   N2 = E2-N1
145   R2 = N2/D2
150   X1 = (XO-R2)
152   PRINT X1,N2
155   V = ABS (XO-X1)
160   IF V < 1.0E-3 GO TO 190
170   XO = X1
180   GO TO 30
190   R = X1
200   PRINT R
210   STOP
```

I.E PROGRAM TO FIND EMISSION RATE CONSTANTS BY AREA METHOD

```
  5   E1 = 583,  E2 = 1003
 10   M=3
 12   H = 2.4414E-6
 15   J = E1,  P=E2-1, K=1, E=0,    = 0
 17   F1 = B(M,O,E1)+B(M,O,E2)
 25   IF K=(INT(K/2))*2 GO TO 50
 30      =    + B(M,O,J)
 40   GO TO 55
 50   E = E+B(M,O,J)
 55   J = J+1, K=K+1
 60   IF J < = P GO TO 25
 65   PRINT 'E', E, '  ' ,
 67   PRINT 'F1', F1
 70   S = (F1+2*E+4*  ) * (H/3.0)
 80   PRINT S
 90   K = ABS (S)
100   M1= B(M,O,E1)
```

```
200    D(L,M)=P1/B(K,O,E3)
210    M = M+1
220    NEXT K
230    L = L+1
235    PR. 'N1', N1
240    IF E2 < = E4 GO TO 270
250    N1 = N1-1
260    GO TO 280
270    IF N1 > =2 GO TO 120
275    IF N1=1 GO TO 355
280    IF N1=0, GO TO 370
290        FOR M1=1
295    PRINT J
300    FREAD (M1,J)
310    J=J+1
320    NEXT M1
330    L=1
340    E1=132, E3=119
350    E4=364, M=9
360    GO TO 130
370    S = 1
380    PR. 'WINDOW', W(S)
390    FOR N=1 TO 12
391    S5=0
392    FOR S2=1 TO  150
394    S5 = S5+1
396    NEXT S2
400    PR. N,D(S,N)
420    NEXT N
430    S = S+1
440    IF S < = L GO TO 380
450    STOP
```

APPENDIX II

PROGRAM TO FIND MULTIEXPONENTS IN A DECAY TRANSIENT FROM
RELAXATION STUDY

```
10 REM **********
20 REM PROG. FOR MULTIEXPONENTS
30 REM **********
40 DIM X(100), Y(100)
45 DIM Z(225),T(225)
50 X(1) = 1.000: X(2)=0.9902145: X(3)=0.9619537
   X(4) = 0.9182789.
60 X(5) = 0.8633796: X(6) = 0.8016901: X(7) = 0.7371572
   X(8) = 0.6728157
70 X(9) = 0.61081 : X(10) = 0.5523: X(11) = 0.4980:
   X(12) = 0.4480.
80 X(13) = 0.4022: X(14) = 0.36036: X(15)= 0.32210
   X(16) = 0.28713
90 X(17) = 0.25513: X(18)= 0.2258: X(19) = 0.19801
   X(20) = 0.17440
100 X(21) = 0.1519: X(22)=0.13138: X(23) = 0.11272
   X(24) = 0.0958
110 X(25) = 0.08055: X(26) = 0.06687: X(27)=0.05470
   X(28) = 0.043925
120 X(29) = 0.03449: X(30) = 0.02631: X(31) = 0.0193(
   X(32) = 0.01335.
```

130 X(33) = 0.00840: X(34)=0.00434: X(35)=0.00109 :
   X(36)= -0.001446.

140 X(37) = -0.00335: X(38)= -0.004713: X(39)= -0.005609:
   X(40) = -0.0061.

150 X(41) = -0.006305: X(42)= -0.006239: X(43)= -0.005978

160 X(44) = -0.005572: X(45)= -0.00506: X(46)= -0.0045017:
   X(47) = -0.0039079.

170 X(48) = -0.0033124: X(49)= -0.0027360: X(50)= -0.0021946
   X(51)= -0.0017.

180 X(52) = -0.001258: X(53)= -0.00087: X(54)= -0.00549:
   X(55) = -0.0002819.

190 X(56) = -0.0000687: X(57)= -0000946: X(58)= 0.0002131:
   X(59) = 0.0029.

200 X(60) = .0003392: X(61) = .0003588: X(62)= .0003569:
   X(63) = .0003390.

210 X(64) = .0003096: X(65) = .0002729: X(66)= .0002323:
   X(67) = .0001906

220 X(68) = .0001501: X(69) = .000112:

230 X(70) = .0000785: X(71) = .0000493: X(72)= .0000250:
   X(73) = .0000055.

240 X(74) = -.0000093: X(75)= -.0000199: X(76)= -.0000266.

250 X(77) = -.0000303: X(78)= -.0000313: X(79)= -.0000304

260 X(80) = -.0000280: X(81)= -.0000247

270   $Y(1) = 0.0000$: $Y(2)= -0.0368213$: $Y(3)= -.0.108484$:
      $Y(4) = -0.150849$

280   $Y(5) = -.1o145$: $Y(6)= -.1oo64$: $Y(7)= -.20619$:
      $Y(8) = -.20288$.

290   $Y(9) = -.19177$: $Y(10) = -.175144$: $Y(11)= -.1549509$:
      $Y(12) = -.132851$.

300   $Y(13) = -.110161$: $Y(14)= -.087884$: $Y(15)= -.0667373$:
      $Y(16) = -.047204$.

310   $Y(17) = -.0295912$: $Y(18)= -.0140620$: $Y(19)= -.0006752$.

320   $Y(20) = -.010583$: $Y(21) = .019804$: $Y(22)= 0.027107$
      $Y(23) = .0326383$.

330   $Y(24) = .0365665$: $Y(25)= .029067$: $Y(26)= 0.0403226$:
      $Y(27) = 0.0405085$.

340   $Y(28) = .0397995$: $Y(29)= .0383604$: $Y(30)= 0.0363451$:
      $Y(31) = .0338961$.

350   $Y(32) = .0311420$: $Y(33)= .0281976$: $Y(34)= 0.251629$:
      $Y(35) = .0221241$.

360   $Y(36) = .019153$: $Y(37)= .0163071$: $Y(38)= .036326$:
      $Y(39) = .0111631$

370   $Y(40) = .0089212$: $Y(41)= .0069205$: $Y(42)= .0051654$:
      $Y(43) = .0036545$.

380   $Y(44) = .0023793$: $Y(45)= .0013268$: $Y(46)= .0004807$:
      $Y(47) = -.0001781$.

```
390   Y(48) = -.00067: Y(49)= -.0010167: Y(50)= -.0012393:
      Y(51) = -.001358

400   Y(52) = -.0013942: Y(53)= -.0013645: Y(54)= -.0012859.

410   Y(55) = -.0011729: Y(56)= -.0010382: Y(57)= -.0008923

420   Y(58) = -.0007437: Y(59)= -.0005993: Y(60)= -.0004642

430   Y(61) = -.0003418: Y(62)= -.0002343: Y(63)= -.0001429

440   Y(64) = -.0000678: Y(65)= -.0000083: Y(66)= .0000366

450   Y(67) = .0000683: Y(68)= .0000887: Y(69)= .0000996:
      Y(70) = .0001026.

460   Y(71) = .0000997: Y(72)= .0000925: Y(73)= .0000822:
      Y(74) = .0000703

470   Y(75) = .0000577: Y(76)= .0000452

480   Y(77) = .0000335: Y(78) = .0000230: Y(79)= .0000139:
      Y(80) = .0000063:

490   Y(81) = .0000004
500   S1 = 6.01: S2 = 21
502   E2=56: J2=1: X7=0: E1=2.4414E-6
503   E3=105: E4=165: E5=237: E6=393: E7=489: E8=681:
      E9=1065
509   FOR I = 1 TO 10
510   X7 = E1 * I
511   X8 = 100000* X7
512   T(I) = LN(X8)
```

```
513   PR. T(I), B(8,0,I+E2), J2,I
514   Z(I) = X8 * B(8,0,I+E2)
515   J2 = J2+1
517   NEXTI
518   PR.I,J2
520   X7 = E1 * J2
525   X8 = 100000 * X7
530   T(I) = LN(X8)
532   PR.T(I), B(8,0,E2+J2),J2,I
535   Z(I) = X8 * B(8,0,E2 + J2)
540   I = I+1
542   IF J2+E2 < E3 GO TO 580
545   IF J2 + E2<E4 GO TO 590
547   IF J2+E2 < E5 GO TO 600
548   IF J2+E2 < E6 GO TO 610
550   IF J2+E2 < E7 GO TO 620
560   IF J2+E2 < E8 GO TO 630
565   IF J2+E2 < E9 GO TO 640
570   GO TO 650
580   J2 = J2+2: GO TO 520
590   J2= J2+4 : GO TO 520
600   J2 = J2+6: GO TO 520
610   J2 = J2+8: GO TO 520
620   J2 = J2+16: GO TO 520
```

```
630   J2 = J2+32 : GO TO 520

640   J2 = J2+64 : GO TO 520

650   P1 = I-1

660   PR. 'P1', P1

670   U = O: C1 = 1: M=4

680   CHAIN 31
```

## File 31:

```
10    REM ******************************

20    REM CONTINUATION FOR MAIN PROGRAM

30    REM ******************************

35    DIM D(225), E(225)

37    DIM V(100), F(100), G(100), C(100)

38    PR. U . U

40    FOR J = 1 TO P1

50    T3 = Cos(U*T(J)) : T4 = Sin(U*T(J))

60    D(J) = T3*Z(J): E(J) = T4*Z(J)

70    NEXT J

80    B(2,0,C1) = U

90    GOSUB 370

91    S3 = S5

92    FOR J9 = 1 TO P1

94    D(J9) = E(J9)

96    NEXT J9

100   GOBUS 370

105   S4 = S5
```

```
110   C(C1) = S3*(1/(SQR(2*PI)))

120   F(C1) = S4*(1/(SQR (2*PI)))

130   U = U + 0.1

140   C1 = C1+1

150   IF U < S1 GO TO 40

160   FOR K=1 TO 71 S2  (51)

170   D3 = X(K): D4 = Y(K)

180   I2 = ((X(K)) * (X(K))+(Y(K))*(Y(K)))

190   G(K) = ((C(K)*D3) + (F(K)*D4))/I2

200   V(K) = ((F(K) * D3) - (C(K)*D4))/I2

210   NEXT K

220   Y1 = 0: Y2 = 1

222   PR. 'MU', S2/10

225   PR. 'Y', Y1

230   FOR L = 1 TO S2

240   Y6 = COS (Y1 * B(2,0,L))

250   Y7 = SIN (Y1 * B(2,0,L))

260   P4 = Y6 * G(L): P5 = Y7 * V(L)

270   D(L) = (P4+P5)

275   T(L) = B(2,0,L)

280   NEXT L

285   P1 = S2

290   GO SUB 370

300   X9 = (SQR (2/PI)) * S5

305   B(M,0,Y2) = X9/100000  1000

310   X8 = EXP (-Y1)
```

```
312    B(7,0,Y2) = X8
315    PR. X8, X9/100000    1000
320    Y1 = Y1+0.1: Y2 = Y2+1
330    IF Y1 < = 9.01 GO TO 225    /0·01
340    S2 = S2 + 20
350    IF S2 >=62 GO TO 363    72
355    M = M+1 : PR. 'M', M
360    GO TO 220    160
363    STOP
370    REM ***********************
380    REM NUMERICAL/INTEGRATION ROUTINE
390    REM *****************************
400    E5=0: O5=0    15:0'
405    PR. 'P1', P1
410    J5 = 2: P5 = P1-1:N=1
420    D8 = T(J5+1) -T(J5)
430    F5 = D(1) + D(P1)
440    IF N=(INT(N/2))*2 GO TO 470
450    O5 = O5+D(J5)
460    GO TO 480
470    E5=E5+D(J5)
480    J5=J5+1: N=N+1
490    IF J5<=P5 GO TO 440
500    S5 = (F5+2*E5+4*O5)*(D8/3.0)
510    PR. 'INT', S5
520    RETURN
```

APPENDIX III

This briefly explains the various quantities, which are shown in each of the plots given in the various chapters. A plot can display a single waveform as shown in Fig. 5.6(a) or (b). Or display two waveforms one superimposed upon the other as in Fig. 5.2(a) or (b) or two waveforms, in which there is one displayed above and other below as depicted in Fig. 5.8(a) or (b). In the case where only a single waveform is shown, the values are displayed above the plot and where more two waveforms are used, the quantities pertaining to both are separately shown, one above the plot and other below the plot. The values of these quantities are shown with the help of a cursor and in the plots, the this is the third line For illustration, a typical plot in Fig. A is given, showing two waveforms, one above and other below. The plot at the right, in particular, is chosen and the description for each of the quantities is given. The six quantities above this plot refer to the upper signal waveform and three quantities below the plot show the values for lower waveform. The description of these is as follows:
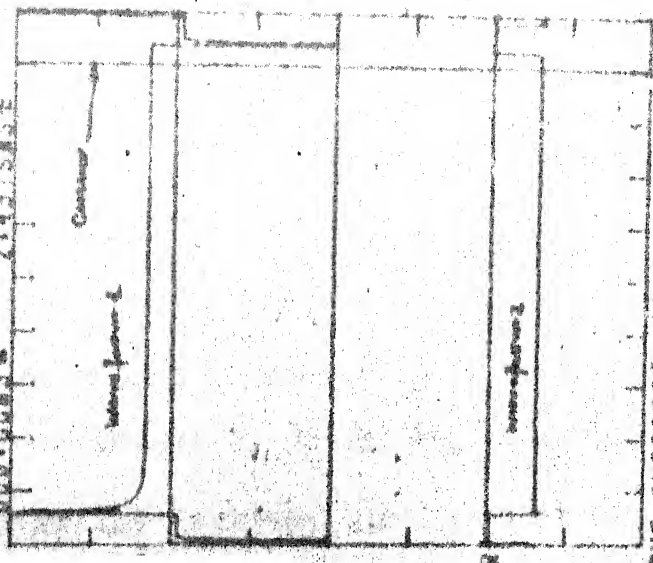
a : This refers to the analysis operation done to get the waveform. In our case, since averaging was done to get cleaner singal, acquired in channel 1, therefore 'CH1 AVERAGE' is printed in that place.
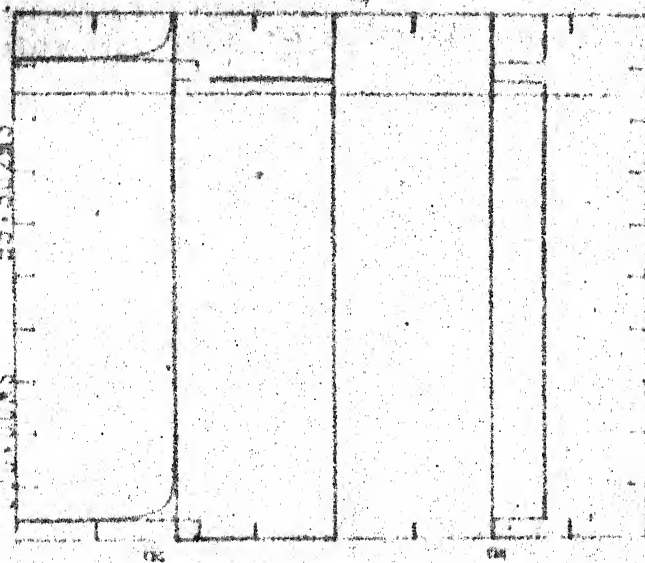
Fig. A

b : This gives the number of such averagings done to get the two waveforms.

c : This refers to the amplitude of the waveform at the point where cursor is placed. This is seen to be 391.60 m REF or mV.

d : This refers to the time instant on the waveform at which the cursor refers to the value in c.

e : This gives the starting time instant of the plot and always shows it as 000.00 msec.

f : This gives the total time to which the signal acquired is displayed. Thus '2.4975 ms' means that signals shown are only upto that time instant.

g : This pertains to the lower second signal, which was acquired in channel 2 through averaging operation. Hence the name 'CH2 AVERAGE'.

h : This gives the amplitude of the lower waveform at the cursor point.

i : The time instant at which the value of h is given is displayed in this.

This completes our description of the plots.

# BIBLIOGRAPHY

1. Sohrab K. Gandhi, 'The theory and practice of micro-electronics', John Wiley and Sons, 1968.

2. P. Braunlich Ed., 'Thermally stimulated relaxation in solids', vol. 37, Springer Verlag, 1979.

3. C.T. Sah, L. Forbes, L.L. Rosier and A.F. Tasch Jr., 'Thermal and optical emission and capture rates and cross-sections of electrons and holes at imperfection centers in semiconductors from photo and dark junction current and capacitance experiments', Solid State Electronics, vol. 13, pp. 759-788, 1970.

4. Judith A., Borsuk and Richard. M. Swanson, 'Current Transient spectroscopy: A high sensitivity DLTS system', IEEE Trans. on Electron Devices, vol. ED-27, No. 12, pp. 2217-2225, Dec. 1980.

5. Lang D.V., 'Deep level transient spectroscopy: A new method to characterize traps in semiconductors', Jr. of Appl. Physics, vol. 45, No. 7, pp. 3023-3032, July, 1974.

6. White A.M., B. Day and A.J. Grant, 'The effect of non-exponential transients on determination of deep level activation energies by DLTS', Journal of Physics 'C', vol. 12, pp. 4833-38, 1979.

7. L.F. Eastman, Kirchner P.D., W.J. Schaff and G.N. Marcas, 'The analysis of exponential and nonexponential transients in DLTS', Journal of Appl. Physics, vol. 52, pp. 6462-6470, Nov. 1981.

8. Wagner E.L., Don Hiller and Dan E. Mars, 'Fast digital apparatus for capacitance transient analysis', Review Scientific Instruments, vol. 51(9), pp. 1205-1211, Sept. 1980.

9. W.M. Bullis, 'Properties of Gold in Silicon', Solid State Electronics, vol. 9(2), pp. 143-168, 1966.

10. D.V. Lang, H.G. Grimmeiss, E. Meijer and M. Jaras, 'Complex nature of Gold related deep levels in silicon', Physics Rev. 'B', vol. 22, No. 7, Oct. 1980.

11. Lanczos C., 'Applied Analysis', Prentice Hall Inc. 196

12. Gardner J.G., J.C. Gardner, G. Laush and W.W. Meinke, 'Method for the analysis of multi-component exponential decay curves', Journal of Chem. Physics, vol. 3, No. 4, Oct. 1959.

13. Bosshart W.C., 'Printed Circuits Boards, CEDT', Tata McGrawhill.

14. Krishnan K.S., 'Waveform Processor based current transient spectroscopy', M.Tech. thesis, IIT Kanpur, 1983.

15. Abramov A.A., 'Tables of ln [Z] for complex argument', Pergaman Press, 1960.

16. Wu and Peaker, 'Capture cross-sections of the Gold donor and acceptor states in n-type Czochalski silicon' Solid state Electrons, vol. 25, No. 7, pp. 643-649, 1982.

EE-1984-M-RAZ-STU